

FUNDAMENTALS OF ULTRASONIC TREATMENT OF ALUMINUM ALLOYS

Raquel F. Jaime, Carl Söderhjelm and Diran Apelian 

Advanced Casting Research Center (ACRC), University of California, Irvine, California 92697, USA

Hélder Puga

CMEMS, University of Minho, Guimarães, Portugal

Miodrag Prokic

MPI Interconsulting, Le Locle, Switzerland

Copyright © 2024 The Author(s)

<https://doi.org/10.1007/s40962-023-01253-w>

Abstract

High integrity cast aluminum components require the use of molten metal processing technologies prior to casting. These include processes such as degassing to reduce porosity, filtration to reduce inclusion content, addition of grain refiners to refine the grain structure, and the addition of chemical modifiers to alter the morphology of eutectic phases. Ultrasonic treatment (UST) is a novel processing method through which ultrasonic energy is introduced into molten metal for the purpose of degassing as well as modifying the cast microstructure. To optimize the use and applications of UST, it is necessary to examine the fundamental mechanisms and the limiting values of

controlling parameters. The effectiveness of UST to perform a desired application within a molten metal is highly dependent on temperature, volume of liquid metal, and the state of the frequency in use. The mechanisms of ultrasonic energy imparted within molten metal will be discussed as well as the benefits of UST during molten metal processing.

Keywords: ultrasonic treatment, degassing, grain refinement, intermetallic morphology modification, aluminum, ultrasonic equipment, Multi-Frequency Mode Modulated (MMM) technology

Introduction to Ultrasonic Treatment of Molten Aluminum Alloys

Aluminum (Al) alloy castings are essential in various applications where high strength, high fracture toughness, and lightweight parts are needed.¹⁻⁵ There are multiple refinement processes and procedures that are applied to molten Al to enhance the mechanical behavior of the cast metal. Some common practices include rotary degassing, the addition of grain refiners such as TiB₂, and the addition of alloy-specific elements which can modify the morphology of intermetallic compounds molten metal (melt) processing technologies target inclusion content, porosity, hydrogen content, grain morphology, and intermetallic morphology. Ultrasonic treatment has shown the potential to enact changes in all these quality detractors.

Ultrasonic treatment (UST) is a processing method through which ultrasonic vibrations are applied to molten metal to enact microstructural change. The ultrasonic waves themselves result in physical changes within the molten metal which affect the solidification behavior, leading to changes in the microstructure.

Ultrasound is a sound wave that oscillates around an equilibrium position. There are two parameters that define this motion around the equilibrium position: frequency and amplitude. Frequency is the wave period per time, or the sound wave travel from peak to peak. The amplitude is the distance vertically from the equilibrium position. Figure 1 displays both frequency and amplitude in relation to wave shape.

Ultrasonic treatment of metal occurs within the frequency range of 18 to 22 kHz, and the most crucial part of a sound wave is the amplitude. The amplitude of the wave directly

Received: 31 October 2023 / Accepted: 18 December 2023

Published online: 27 January 2024

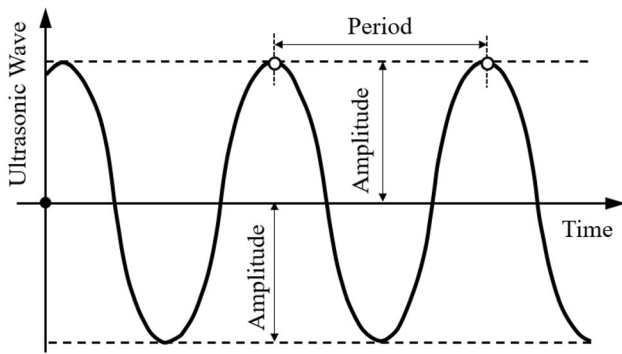


Figure 1. A visualization of a sound wave labeled with an equilibrium position, period (T), and amplitude (A).

relates to the intensity of the treatment applied, seen in Eq. (1).⁶ Intensity is proportional to the square of the initial amplitude, A_0 (μm), and is also dependent on the variables c (m/s), speed of sound, ρ (kg/m^3), medium density, and ω (rad), angular frequency. Density is a measure of how closely packed atoms are within a medium and dictates the efficiency of atoms at communicating and transmitting an ultrasonic wave through the medium. Therefore, a higher density material experiences a higher intensity wave. However, increasing the density of a medium also increases the effects of loss.

$$\text{Intensity} = \frac{\text{Power}}{\text{Area}} = \frac{1}{2}c\rho(\omega A_0)^2 \quad \text{Eqn. 1}$$

An ultrasonic wave travels through a medium with a repeating unit oscillation per time, frequency, and an amplitude that oscillates equally above and below the equilibrium. This frequency and amplitude repeat indefinitely at the same magnitude in a theoretically friction-free environment. Realistically, both the frequency and amplitude decay because of losses and acoustic loading conditions in the medium. The total loss in the medium is termed attenuation. Attenuation is the gradual loss of ultrasonic energy due to the combination of reflection, refraction, and absorption. Absorption is the sudden loss due to the wave affecting the medium and expending energy for a material response. Reflection and refraction result from the wave encountering an obstacle and are therefore less predictable than absorption. These forms of losses cause decay in both frequency and amplitude of the wave.⁶

Although both parameters experience decay, amplitude decay is what leads to decay in intensity. Ultrasonic equipment directly supplies frequency, so amplitude decay is the issue with maintaining the wave.⁶ Amplitude decay from the total loss of attenuation is shown mathematically in Eq. (2) where A is the new decayed amplitude value, A_0 is the initial amplitude, δ is the medium constant attenuation factor, and t is the time that has passed.⁶ Amplitude decay can be found in direct relation to absorption as in

Eq. (3) where α is the medium absorption factor constant, and x is the wave path distance.⁶ The loss and absorption of a wave result from its interaction with the medium, hindering its ability to travel along the medium in which it is being transmitted. If there was no loss, then the wave would have no energy expense on the medium and therefore no effect.

$$A = A_0 e^{-\delta t} \left(\cos \sqrt{\omega_0^2 - \delta^2} t \right) \quad \text{Eqn. 2}$$

$$A = A_0 e^{-\alpha x} \quad \text{Eqn. 3}$$

A wave traveling through the medium experiences both reflection and refraction, which causes the ultrasonic wave to be composed of both traveling and standing waves. Traveling waves are oscillations with all energy moving in one direction. Two traveling waves that move in opposite directions superimpose to produce a standing wave due to the reflection of the initial wave and equal energy in both the forward and reverse directions. Due to the movement of energy in both directions, a standing wave oscillates with double the amplitude of its equal traveling wave counterpart. This effect is visualized in Figure 2 where two traveling waves compile to produce a larger standing wave. The traveling wave experiences attenuation and absorption throughout the medium, and the standing component is produced from reflection and some refraction.

An ultrasonic wave traveling through a medium is a loaded wave and can be described in three ways; free, dampened, and forced. A free, or natural, wave is one that continues with constant frequency and constant amplitude without an external force. A dampened wave is one that experiences decay, such as attenuation and absorption, as it continues through a medium, resulting in a decrease in amplitude and frequency. A forced wave is one that experiences damping but maintains constant amplitude and frequency due to an added external force, such as an opposing or reflecting wave that is supplementing the amplitude with the production of a standing wave. Free waves exist theoretically when there is nothing to dampen the wave or create losses. Ultrasonic waves that travel through metal melts exist as either dampened or forced.

Mechanisms of Ultrasonic Treatment in Molten Metals

The mechanisms by which ultrasonic waves interact with molten metal and bring about modifications to the metallurgical quality of the metal can be categorized as either via cavitation and/or streaming. These are further detailed out below.

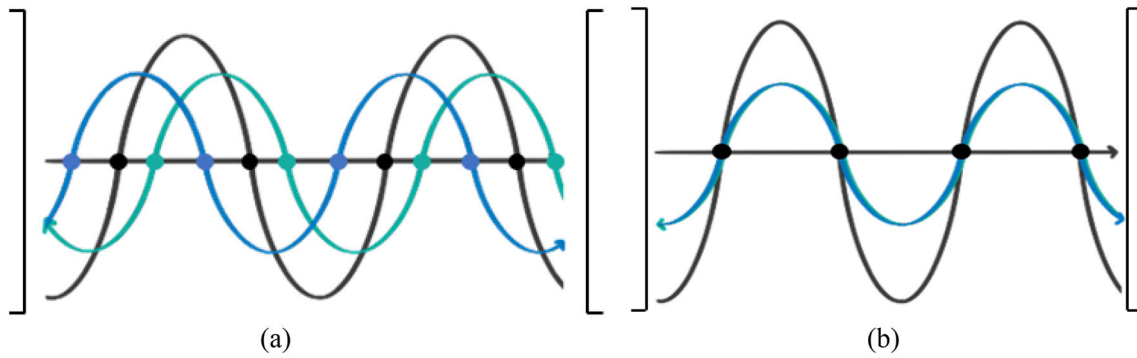


Figure 2. A blue traveling wave moving right and a green traveling wave moving left superimpose themselves, producing a gray standing wave (a), two traveling waves fully superimpose to produce a gray standing wave with double the amplitude (b).

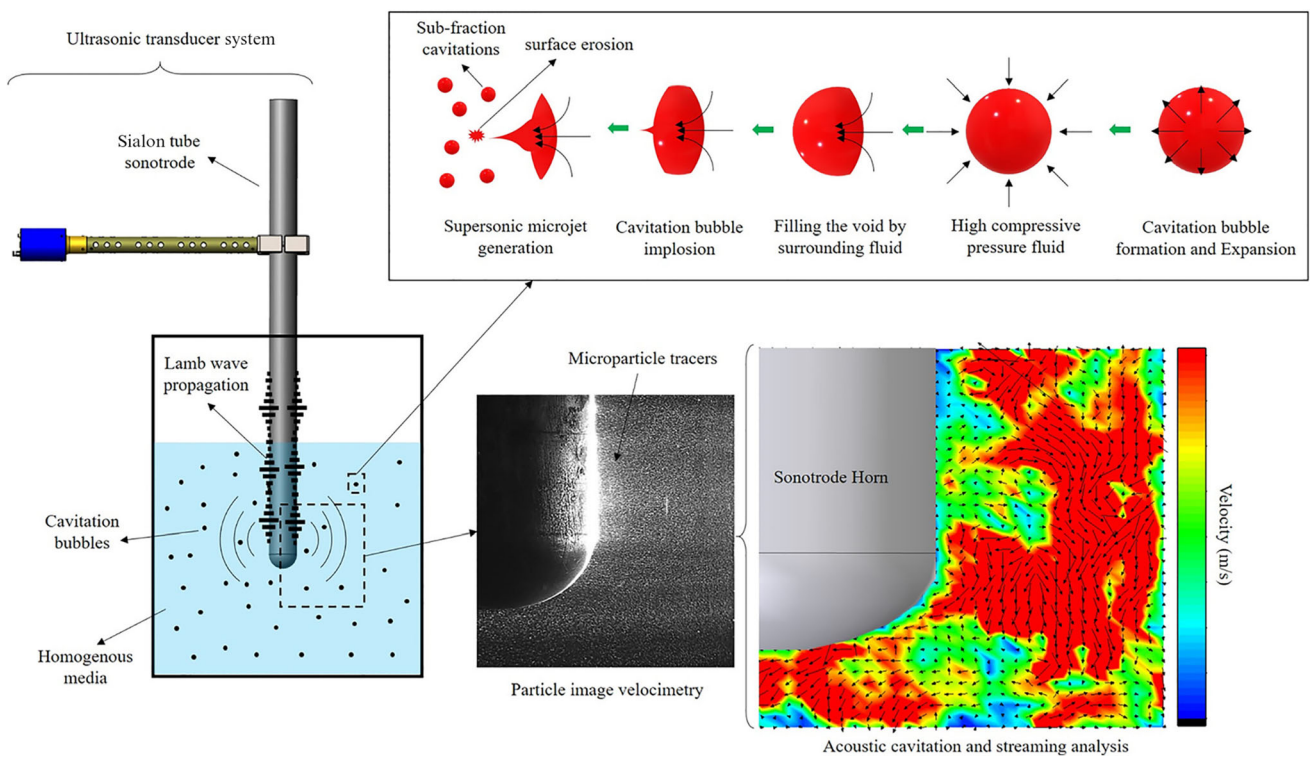


Figure 3. A visual representation illustrating how an ultrasonic wave generates compression and rarefaction, leading to acoustic cavitation.

Acoustic Cavitation

In liquid media, the peaks of an oscillating ultrasonic wave result in two actions, compression, and rarefaction. During compression, the wave causes bubbles and gas to compress and pressurize. As oscillation continues, rarefaction sets in and causes tensile stresses within the medium. Any existing bubbles expand, and the tensile stresses form new cavities that experience compression and rarefaction in the oscillations to come. With each passing oscillation the bubbles compress more and expand more than the previous oscillation. Eventually, the bubble reaches an unstable size and shape so that on the successive compression stage the

bubble collapses, Figure 3. Upon collapse, the surrounding material experiences hydraulic shockwaves with local pressures of thousands of MPa and local temperatures of up to 5000 °C.⁶ If the temperature is below the liquidus, the shockwave of acoustic cavitation can lead to dendrite fragmentation which will cause in situ grain refinement.⁷ In the liquid state, this mechanism results in increased mass transport due to the turbulence of cavitation.⁸

Acoustic cavitation is an intensity dependent mechanism.⁹ During a low intensity treatment, the wave functions in a “pre-cavitation” mode in that bubbles form, compress, and rarefaction is occurring, however, the bubbles do not

collapse. There is a cavitation threshold value that is material specific and depends on the ultrasonic wave intensity; below the cavitation threshold is when the bubbles do not collapse, the “pre-cavitation” mode. This mode can occur at both low and high frequencies; intensity is dependent on the frequency—Eq. (1). At low frequencies, the intensity is insufficient and there is not enough power per surface area to cause the bubbles to reach that unstable shape and size for collapse. At high frequencies, the intensity is sufficient, but the oscillation period is not long enough for the bubble to collapse. In this case the bubbles are supplied with enough power to reach an unstable size, but before collapse can occur the bubble is already entering the next stage of rarefaction. Pre-cavitation in the liquid state leads to bubble formation and aggregation, and subsequently the bubbles rise to the surface and escape the melt (degassing).

Cavitation bubbles grow in predictable locations known as cavitation nuclei. Cavitation nuclei grow at “weak points” in the liquid medium where there is a difference in surface tension or separation of material. The interface between two immiscible liquids, the complex surfaces of particles, and other gases or insoluble impurities are examples of cavitation nuclei. These interfaces and surfaces become weak points because they have a low wettability in liquid Al. Due to their low wettability, these locations have a high propensity for hydrogen collection. Aluminum oxide, Al_2O_3 , is pervasive in all molten Al processing, and the oxide mixes into the melt volume and has poor wettability with the melt. Hydrogen adsorbs on the surfaces of these oxide particles. Within a given melt of liquid aluminum, 0.005 % of Al_2O_3 particles control about 5 % of all dissolved hydrogen in the volume via this mechanism.⁶ When ultrasonic treatment is applied, the adsorbed hydrogen is influenced by the oscillation into cavitation.

Acoustic Streaming

Acoustic streaming occurs in two ways: (i) streams that form directly due to the ultrasonic energy absorption, and (ii) streams following the collapse of bubbles from acoustic cavitation. As ultrasonic energy is absorbed by the melt, streams form in viscous layers near solid boundaries or phase interfaces in fields of standing waves away from the boundary layers; streams form from the absorption of wave momentum. After the collapse of a bubble caused by acoustic cavitation, the streams that form cause liquid material to rush into the regions where the bubble imploded with velocities of hundreds of m/s. Streams that result directly from the energy of an ultrasonic wave are slower than those of acoustic cavitation, but these streams are sped up once cavitation sets in. Acoustic streams form closed loops whose size is inversely proportional to the acting wave’s frequency.⁶ The combination of the high temperature and high pressure of acoustic cavitation with the high

velocity travel of acoustic streaming results in a homogeneous distribution of material and temperature. During continual operation, the streaming loops combine and form larger homogeneous loops that orientate themselves lengthwise in an oval shape from the ultrasonic source, Figure 4. In the liquid state, both stream types result in increased mass transport along these stream loops.⁸ In the liquid-solid state, the streams impact solidifying surfaces and result in surface damage or dendritic fragmentation, after which these fragments can be transported as new nuclei for heterogeneous nucleation.

Ultrasonic Instrumentation and Considerations

There are five main parts involved in the production of an ultrasonic wave; an ultrasonic generator, a transducer, a waveguide, booster, and a probe. These components are further discussed.

Ultrasonic Generator

The ultrasonic generator converts electricity into voltage pulses that are required for the transducer. The controls on an ultrasonic generator are power, frequency, and amplitude. In terms of ultrasonic treatment of molten metals, the power range varies from 200 to 2000 watts depending on the emitting face area. For larger areas, higher power is required and vice versa. Frequency of ultrasonic treatment occurs most effectively within the range of 18–22 kHz. Low frequencies do not supply enough intensity for treatment to occur. High frequencies do not allow enough time for the treatment to have a lasting effect.⁶ On an ultrasonic generator, frequency is directly supported by the power and therefore the amplitude is what experiences decay. In general, there is no relationship between amplitude and frequency and an ultrasonic wave can have any amplitude. However, in a working relationship of both frequency and amplitude being produced by the same power source, the amplitude can only be so high before adversely affecting the frequency and vice versa. Many ultrasonic generators have a fixed frequency tracking, and the amplitude is tuned on a scale of 0 to 100% where the amplitude can be set as a percentage of the maximum. The maximum value is determined by the system’s setup such as the material, shape, and size of the emission equipment.

Transducer

Electricity is supplied from the ultrasonic generator to the transducer in the form of voltage and current pulses. In the transducer these electric pulses are converted to mechanical energy, also known as ultrasonic vibration. There are two commonly used transducer types, magnetostrictive and piezoelectric.

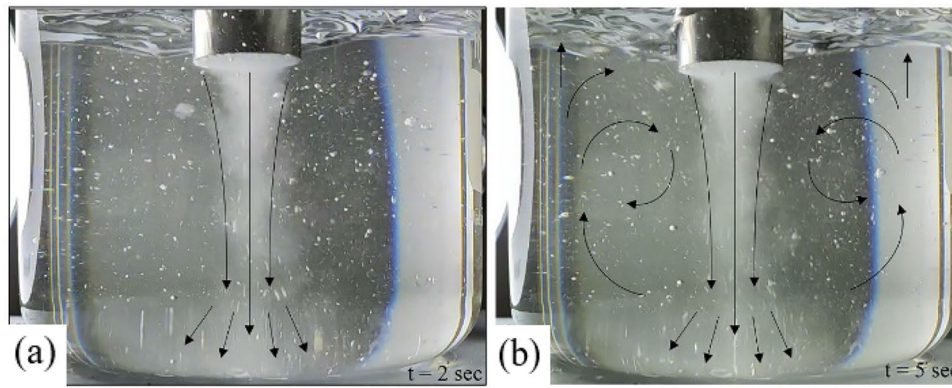


Figure 4. The formation pattern of acoustic streaming loops in relation to the location of the ultrasonic source at $t=2$ seconds (a) and $t=5$ seconds (b).

The magnetostrictive transducer (MST) was first used in ultrasonic treatment of metals through feeders and molds.⁶ Magnetostriction is the process that converts magnetic field energy to mechanical energy. The basic assembly of an MST is a magnet layered over a meander coil layered over a magnetostrictive patch of a select material, most commonly FeCoW alloy.¹⁰ This assembly connects to a transformer, waveguide, booster, and radiating surface that is in direct contact with the melt. MSTs connect to an ultrasonic generator that supplies a DC current for magnetization and an AC current for excitation. MSTs function with a supplied current that induces both permanent and variable magnetic fluxes in FeCoW. The high magnetostrictive coefficient of FeCoW causes the patch to change dimensions in resonance with the frequency of the AC current of excitation. This flux in size of the material induces longitudinal oscillations within the material that are transmitted to the transformer, then to the waveguide, and via the radiating surface into the melt. A drawback with magnetostrictive transducers is that they require a water-cooling system on the meander coil which proves challenging in molten metal applications.

Piezoelectric transducers function on piezoelectric materials. A piezoelectric material retains the property to convert electrical energy into mechanical energy and vice versa. The piezoelectric transducer is supplied with voltage pulses from the ultrasonic generator, those pulses create an electric potential under which the piezoelectric material—commonly lead zirconate titanate (PZT)—mechanically deforms and produces a vibration.¹¹ Piezoelectric transducers operate in two regimes, parallel resonance which is voltage driven, and series resonance which is current driven. Piezoelectric transducers are more common and are used in ultrasonic treatment of metals due to their simple design and ability to run without water-cooling and rely on air-cooling.

Waveguide

The purpose of a waveguide is to direct the ultrasonic wave from the transducer to the booster or directly to the probe.

The waveguide operates to maintain the intensity of the wave and transmit it with minimal losses. A waveguide may be involved in the equipment design for the purpose of functionality due to the spatial and thermal separation of the transducer and the probe.

Booster

The booster is designed to increase or decrease the amplitude and pressure of a wave. The booster may be designed to transmit the wave functionally from the transducer to the probe, but the primary purpose is to adjust the intensity of the wave. As the oscillatory amplitude is amplified, the radiated oscillatory pressure is reduced. Similarly, as the oscillatory amplitude is reduced, the radiated oscillatory pressure is increased. A booster may be required to match the impedance of the transducer to the probe. Impedance is a material specific property that affects the oscillation through contact. Equation (4) shows how impedance can be calculated from ρ , material density, c , speed of sound, and s , contact surface (m^2).⁶ Similar to how an electrical transformer adjusts for the best ratio of voltage to current, the waveguide adjusts for the best ratio of motion to pressure for the traveling wave by matching the impedances of these equipment components.⁹

$$z = \rho \cdot c \cdot s \quad \text{Eqn. 4}$$

Probe

Now that the wave has been produced by the transducer and optimized by the waveguide and booster, the oscillation is transferred to the probe, sometimes referred to as the ultrasonic horn, or sonotrode. The function of the probe is to transmit the wave directly into the medium, or liquid metal. Probe design depends on three key parameters: geometry, material, and vibration modes.

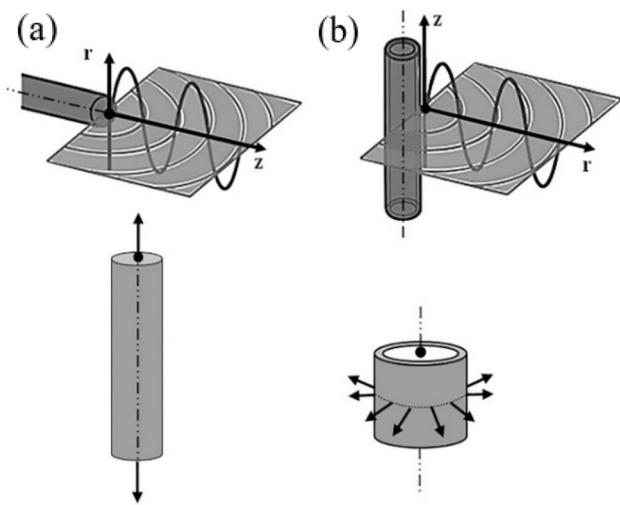


Figure 5. Solid probe sound wave emission (a) and hollow probe sound wave emission (b).

In terms of geometry, oscillations are emitted longitudinally from the faces of the probe. Traditionally, probes are solid made in metallic material, and the oscillation is emitted perpendicular to the contact face, as illustrated in Figure 5. In this case, the solid probe is only immersed in the liquid metal to a depth of less than 5% of the total length, typically 10–15 mm to maintain a resonant frequency (and avoid overloading).^{12,13} In contrast, in a hollow probe, usually in a ceramic material, oscillations can be emitted perpendicular to the longitudinal axis of the probe, as depicted in Figs. 5, 6 and 7. Hollow probes come in two variations: one with one end closed and the other with both ends open. For a hollow probe with one end closed, the generated acoustic power is high, and the acoustic field is predominantly radial.¹⁴ Such a probe can be submerged in the liquid mass to a depth of up to 30 % of the total length (Figure 6). On the other hand, for probes with both ends open, the acoustic field propagates radially and axially, resulting in lower acoustic power. In this case, it is recommended to insert the probe to a maximum depth of 5 to 10 % of the total length (Figure 7).

Metallic probes are commonly made of titanium, aluminum, and sometimes refractory metals such as niobium. Niobium probes are chosen for their high temperature resistance. However, Niobium probes cannot withstand amplitudes greater than 10 μm and undergo erosion over time. Moreover, niobium is not cost-efficient. Aluminum is sometimes used as a probe because it is an inexpensive option; however, it must be coated with nickel or chrome to increase wear-resistance and working temperature. This option is not viable as the probe and coating erode with time. Titanium, Ti-6Al-4V, is the most common choice for metallic probes due to its relatively high melting point and mechanical toughness to withstand fracture from high frequencies. The major drawback to metallic probes is that the prolonged use of applying an ultrasonic frequency

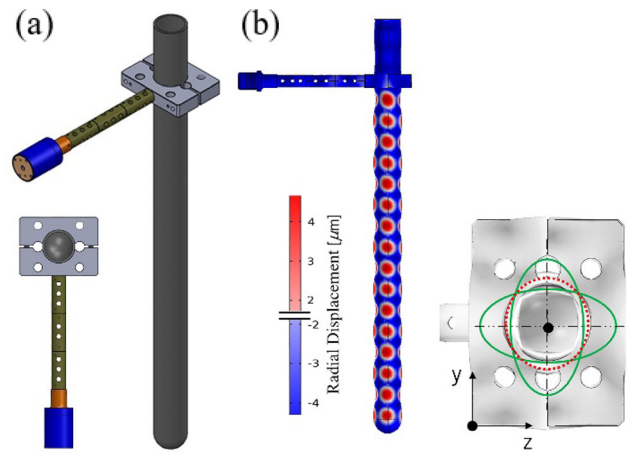


Figure 6. Hollow SiAlON Sonotrode, one end open (a) and the direction of displacement radially (b).

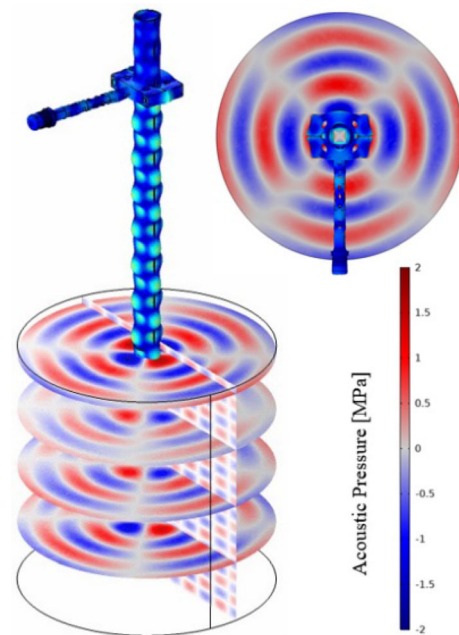


Figure 7. Concept of SiAlON Sonotrode with both ends open designed to resonate at radial eigenmode (concept created by H. Puga and Miodrag Prokic).

result in material erosion and potential contamination of the melt.¹⁵ Ceramic materials are a good choice for ultrasonic probes to be used for molten metal processing.¹⁶ SiAlON is a ceramic developed in the 1970s consisting of silicon, aluminum, oxygen, and nitrogen. For ultrasonic probe applications, β -SiAlON is used due to its excellent fracture toughness. β -SiAlON has the chemical formula $\text{Si}_6\text{-zAl}_z\text{O}_z\text{N}_{8\text{-z}}$ where z ranges from 0 to 0.42.¹⁷ The fracture toughness of β -SiAlON is $7.7 \text{ MPa} \cdot \text{m}^{1/2}$ which is higher than alumina at $4.5 \text{ MPa} \cdot \text{m}^{1/2}$.¹⁸ Although this fracture toughness is not as high as titanium or other metallic options which range around $30 \text{ MPa} \cdot \text{m}^{1/2}$, the wear-resistance of SiAlON is higher and thus it is less likely to erode in the molten metal.¹⁵

The motion (spiral and rotational) of a probe greatly impacts the efficiency of ultrasonic treatment. Ultrasonic waves can only travel so far into the melt and treat a specific volume due to the acoustic attenuation of the wave. Probe movement enables the treatment of larger volumes because the ultrasonic source is brought closer to farther reaches of the melt. Some examples of probe motion have been tested using hollow SiAlON probes where emission occurs at 90 ° angles.¹⁴ When the probe is placed in the center of the liquid metal, it can be spiraled so that the treatment reaches the areas in between the 90 ° intervals. If the probe is placed off center, then the probe can be rotated around the circumference of the liquid metal and can affect the outer edges of the crucible. Alternatively, a combination of both motions - spiral and rotation of the probe may be used. The main issue with using ceramic probes is that they dominantly support radial vibration motion. This type of motion (vibration mode) has a lower amplitude compared to the axial mode, and this is why rotational motion is the preferred method for SiAlON ceramic tubes. As shown in Figure 6, the radial vibration motion induced by the imposed mechanical coupling is elliptical in nature. As a result, the SiAlON probe tends to exhibit 4 planes (90° apart), where the amplitude is at its maximum value. Figure 8 displays a perspective of these motions for hollow sonotrodes.

Equipment and Amplitude

The three main considerations for maximizing amplitude are power supply, probe diameter, and system resonance. The power supplied is directly proportional to the amplitude and intensity of the treatment, as given by Eq. (1).⁶ Probe diameter affects power consumption; the larger the probe diameter is, the more power is required to maintain the amplitude. However, probe diameter is also a function of the volume of melt to be treated, and the maximum

potential amplitude; so, there is a tradeoff between amount of power supplied versus probe diameter. System resonance is determined by a frequency match with the distance to the nearest solid surface. If the frequency of the probe and the nearest solid surface are matched, then the amplitude of the oncoming wave and the reflected wave is constructive and forms a larger amplitude. This resonance is how a system can be configured to address the challenge of attenuation by increasing the amplitude and intensity. When the system is out of resonance, the waves are destructive and can reduce the amplitude to zero resulting in no effective treatment.

Existing Ultrasonic Instrumentation

Southwire

Southwire is a leading manufacturer of wires and cables and of metal processing equipment. A division of Southwire is SCR technologies which has developed ultrasonic degassing equipment for use in launder systems.¹⁹ The generator is a fixed 20 kHz frequency and variable 1500 W AC power supply from Sonics & Materials, Figure 9. This generator works to maintain a constant amplitude of treatment by varying the power supplied. As the viscosity of the molten metal changes during processing, the generator increases the power supplied to ensure the amplitude of the probe is maximized, and that it remains constant. The transducer is piezoelectric and is supplied by Sonics & Materials and is rated to match the generator. The transducer is the topmost part of the sonotrode, followed by the booster and probe. The probe is supplied by Southwire, made of SiAlON ceramic and is 22 mm in diameter. There are three small through-holes that run up the length of the probe so that purge gas can flow through it for the purpose of a combination of UST and purge degassing. Although the Southwire probe was mainly aimed for degassing the

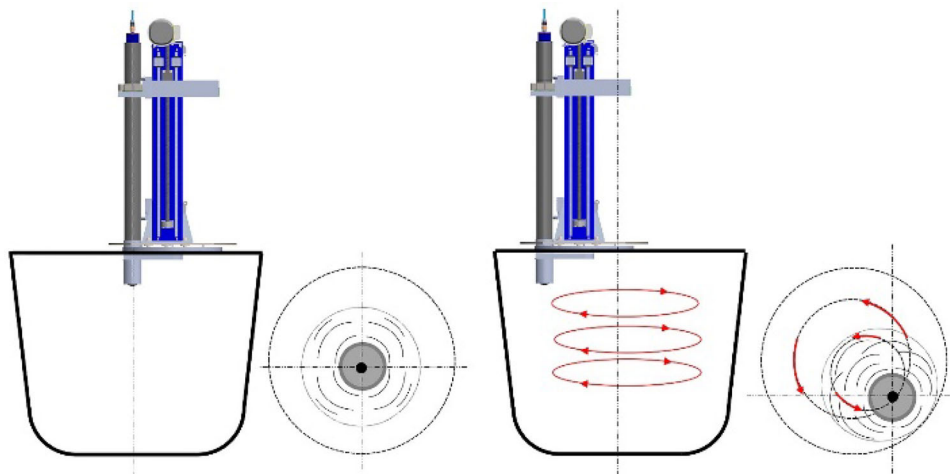


Figure 8. Two distinct types of motion: spiral and rotational, utilizing a Sialon Sonotrode (concept created by H. Puga and Miodrag Prokic).

melt, it is also capable of being used for ultrasonic treatment without purge gas flow for other applications such as grain refinement and intermetallic modification. Figure 9 shows a schematic diagram of the Southwire sonotrode. Southwire also produces larger, industry-scale equipment which uses two generators from Ducane and two adjacent sonotrodes to increase the treatable volume.¹⁹

MP Interconsulting

MP Interconsulting, MPI, is a Switzerland based company that produces ultrasonic equipment for various applications outside of liquid metallurgy. Recently, MPI has developed ultrasonic equipment for foundry applications. Considering ultrasonic physics and science of wave propagation, MPI has developed novel utilization of amplitude and frequency modulation to increase the effectiveness and efficiency of UST for molten metal processing. Their approach operates in a variable frequency modality, which has many advantages over fixed frequency modality. Specifically, the Wideband Multi-Frequency, Multimode, and Modulated (MMM) Ultrasonic Technology, or MMM developed and patented in 2001 (EP1238715A1) by MPI alters the frequency as the probe is operating around the volume of the treated melt.^{18,20} MMM in liquid processing increases effects of cavitation, sonochemistry, and homogenization because standing waves are not created and the total liquid volume is uniformly agitated.¹⁸ MMM is used to optimize the system resonance and to increase the amplitude, as well as altering the frequency when the melt viscosity increases, which occurs as temperature decreases. The basis of MMM modality in UST is to maintain the highest amplitude possible via system resonance. As mentioned previously, amplitude is related to the intensity of the wave which dictates the effectiveness of the ultrasonic wave.⁶ The MPI system operates with a hollow probe which emits ultrasonic waves at 90 ° angles laterally. As the probe rotates around the volume of the melt the frequency supplied

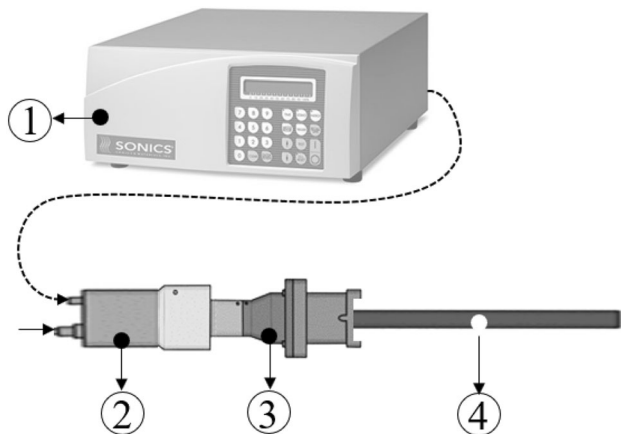


Figure 9. Southwire device. (1) Sonics & Materials ultrasonic generator, (2) PZT Transducer, (3) Booster, and (4) SiAlON Probe.

changes to match the wavelength of treatment to the distance between the probe and nearest solid surface. MMM is operated via software that controls the physical motion of the probe and ultrasonic wave generation. The hollow probe is approximately 1200 mm tall and 80 mm in diameter. The probe can either be one-end-open or both-ends-open depending on the desired treatment (acoustic power vs acoustic field). The probe is connected to a waveguide that runs to the transducer as seen in Figures 6, 10.

Multi-Frequency Effect on Acoustic Cavitation

The combination of two or more ultrasonic sources is proven to increase the acoustic cavitation yield.²¹ Studies that combined ultrasonic sources began with two sources; one in the high-kHz frequency range and one in the low-MHz frequency range. The high-kHz frequency source acts as the main source through which sonication effects occur. The low-MHz frequency source acts as an auxiliary and enhances the sonication effects of the main source. The mechanisms of how this combination increases the cavitation yield is not certain, but there are various ideas promoted in literature. Most theories suggest that the high-kHz frequency agitation is enhanced by the addition of a low-MHz. The low-MHz addition produces more bubbles, decreases the pressure-threshold for cavitation to occur during the negative pressure half-wave, and increases the collapse rate during the positive pressure half-wave. In the study by Feng et al.,²¹ dual and three-frequency irradiation were observed. It was found that adding a third source increases the cavitation yield further. This paper suggests that the increase in irradiation by additional sources may



Figure 10. MPI ultrasonic equipment setup (Photo courtesy of MPI).

break the surface continuity within the liquid and therefore increase the amount of cavitation nuclei where the primary source may form more cavitation bubbles. The combined frequencies may create a sound field where cavitation bubbles should form and collapse for a wider range of nuclei, i.e., the thresholds and required pressure-barriers for acoustic activity are lowered due to an increase in bubble-sound field, bubble-bubble interactions, and an increase in mass transfer.

Acoustic cavitation is the underlying mechanism for all major sonication effects in a liquid.^{6,22} The use of multi-frequency ultrasonics is not only a matter of increasing the cavitation yield, but also of managing control of cavitation such as when and where it occurs. The study by Moholkar et al.²² identifies characteristic parameters of the dual-frequency ultrasonic agitation as α , the dual-frequency ratio, β , the pressure amplitude ratio, and φ the phase difference. This study mathematically set conditions around these parameters to prevent the amplitude from decaying to zero or to below the transient cavitation threshold. This is only satisfied if; the mean difference between the average pressure amplitude and the local pressure amplitude in the region between the ultrasonic sources, $I(\alpha, \beta, \varphi)$, reaches a minimum, and if the acoustic pressure amplitude falls below the transient cavitation threshold near the radiating source and exceeds the cavitation threshold in all other areas. These conditions are met when the phase difference, φ , between the produced ultrasonic waves is $\pi/2$ or $(-\pi)/2$ and when the frequency being coupled is a first sub-harmonic, $\alpha = 0.5$, or is an ultra-harmonic, i.e., $\alpha = 1.5, 2.5, 3.5 \dots$ etc.²². By following conditions with these standards, the cavitation yield can be increased, and the placement of cavitation can be managed. This prevents cavitation from being placed immediately at the radiating source, therefore, preventing damage and erosion of the probe by cavitation.²²

The impartment of multi-frequency ultrasonic waves prevents the existence of standing waves and of nodes. Standing waves in the liquid metal creates a nonuniform method of treatment.²³ As mentioned previously, a standing wave makes for the highest amplitude, but the superposition of two frequencies and amplitudes in this manner creates nodal zones of no treatment. Through standing waves, the liquid metal would receive intense treatment in zones where the wave amplitude peak is, and no treatment in the nodal zones, shown in Figure 11.

Control Systems

In control systems and signal processing, feedback loops are a method of control that allow for adaptation and modification. The phase-locked loop (PLL) is a form of feedback loop which compares the oscillator phase and frequency with a reference.¹⁸ The PLL can produce a

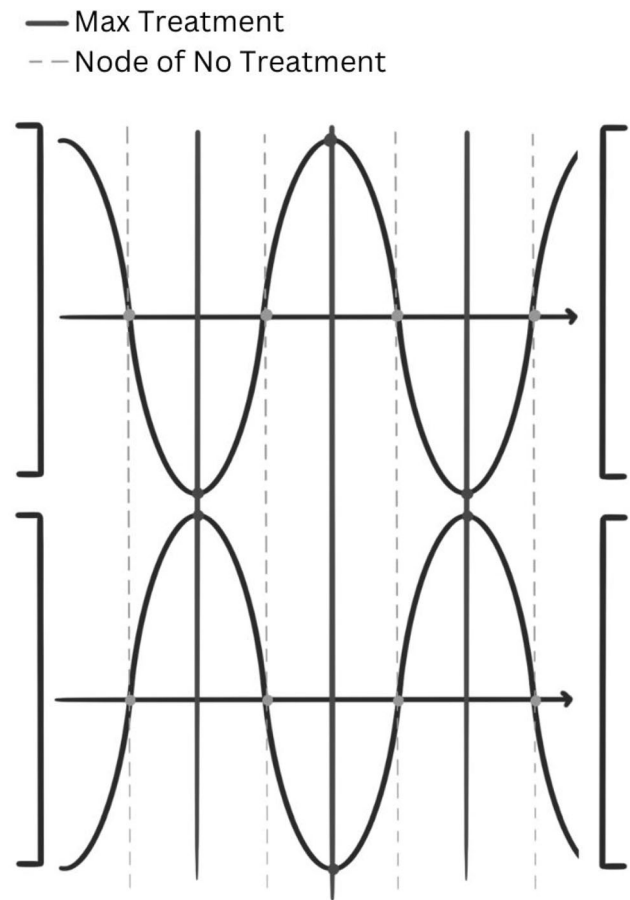


Figure 11. Depiction of the nonuniform treatment that is imparted by a standing wave.

precise frequency based on a reference oscillator. This system utilizes negative feedback and if there is a deviation from the desired frequency, the PLL will adjust accordingly by raising or lowering the frequency to match the reference. The phase does not have to match, although if there are short-term changes to the phase, such as noise, the PLL will adjust accordingly to retain precision.²⁴ As the initial frequency enters the molten metal, the conditions within the load such as the container size, the viscosity, or any inclusions will alter the frequency. The PLL can also assist with synchronization of a primary and secondary ultrasonic source in multi-frequency treatment. In total, the PLL produces a stable and desired frequency in non-stationary conditions.

Along with frequency and phase of an ultrasonic wave, amplitude is another parameter that can be controlled. Pulse width modulation regulates the duty cycle of an ultrasonic wave. The duty cycle of a wave is the percent of the waveform that is above the zero axis. In other words, the duty cycle can be represented by the width of the maximum amplitude of a square wave. The output of a PWM controls the amount of ultrasonic power that is delivered to the load.¹⁸ Power is related to the intensity and thus the amplitude of the ultrasonic wave.⁶ The PWM

varies the duty cycle, or the width of maximum amplitude pulses, to modulate the power of ultrasonic energy delivery. A wider pulse represents a high amplitude signal, delivering more power, while a narrower pulse represents a low amplitude signal, delivering less power.²⁵ PWM can be used in conjunction with forms of feedback loops such as PLL to monitor how the power is affecting the load and whether more or less power should be delivered.

Real-Time Load Parameter Estimation is the process to monitor and estimate the continuously changing parameters of a non-stationary load.¹⁸ For a load under ultrasonic agitation this estimation is determined via the calculated impedance. The two crucial load parameters that determine impedance are current and voltage. Both current and voltage are monitored via their envelope and phase. An envelope is a defined range of values that represents the specific current or voltage levels required by the load.²² These maximum values are recorded by monitoring the load. The ratio of the voltage envelope to the current envelope gives the magnitude of the impedance that is experienced by the load. The impedance of the load is the opposition to an alternating current that results from the combination of the resistance and the reactance that the load experiences. Differences in resistance and reactance lead to phase shifts between the voltage and current. The phase difference between voltage and current gives the argument, or phase-angle, of impedance. Resistance of a load under ultrasonic agitation can be interpreted as the local-changing viscosity of the molten metal with local-changes in temperature or due to the presence of solid inclusions.

Ultrasonic Treatment Applications

At the onset, it is important to distinguish between ultrasonic treatment (UST) by the temperature of the metal or the medium. Ultrasonic treatment is either carried out in the fully molten state (above the liquidus), or slightly below the liquidus temperature (5–10% fraction solid), and if appropriate probes are utilized, at temperatures in the mushy zone (10–20% fraction solid). Degassing and mixing for metal matrix nanocomposites are possible in the fully liquid state while grain refinement and intermetallic modification occur with some amount of fraction solid. Figure 12 displays the temperature ranges that work successfully for their respective UST applications.

When treatment is applied above the liquidus temperature, the dominant effect of the ultrasonic energy is the creation of cavitation bubbles and large streaming loops which encompass the entirety of the treatable volume. The combination of these two effects results in UST being an efficient degassing technique. As the temperature lowers and approaches the liquidus temperature, UST streaming loops are flowing to homogenize the composition all the way to

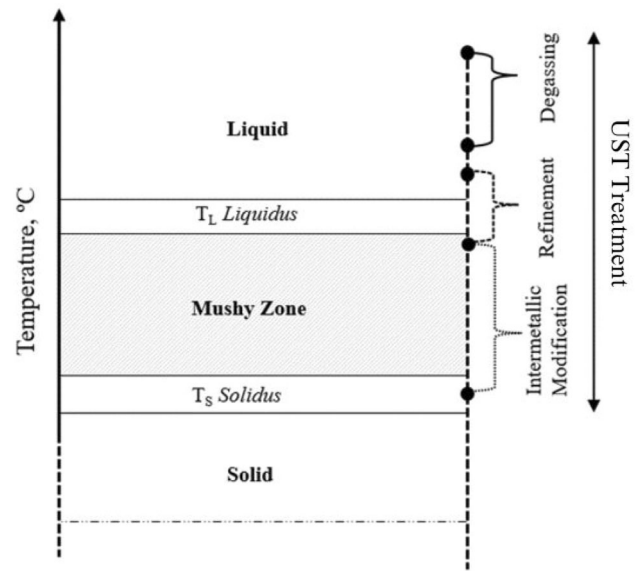


Figure 12. Preferential treatment temperature ranges for UST degassing, grain refinement, and intermetallic modification.

the onset of solidification. This effect alters the formation and the morphology of the first solidifying phases, which can be beneficial in modifying the morphology of iron-based intermetallic phases. The cavitation bubbles and streaming loops that are formed via ultrasonic energy impact the solidified interfaces and cause fragmentation. The fragmented particles are redistributed by the streaming loops and act as nucleation sites in new locations and thus in situ grain refinement.^{26,27} Grain refinement may also be attained in the fully liquid state via broken oxides rather than fragmented solidified phases.

Degassing

The solubility of hydrogen in molten Al is $\sim 0.7\text{--}0.8$ mL/100 g versus 0.05 mL/100 g in the solid state. If the hydrogen is not removed from the molten metal before solidification, gas porosity significantly impairs the resultant mechanical properties.^{28,29} Trapped hydrogen within the solidified metal exists in the form of porosity.³⁰ Pores in the solidified casts act as weak points for fracture and failure, as do inclusions and oxides. Figure 13 shows the effect of degassing on porosity and the correlation of porosity to ultimate tensile strength in Al-4.5%Cu, Al-11%Mg, and Al-5%Si. As the porosity percentage increases, the ultimate tensile strength decreases.³¹

Accordingly, a key molten metal processing technology for Al is degassing.³² The procedure involves an inert purge gas, such as argon or nitrogen, that bubbles into the lower portion of the melt through a rotating impellor. The rotating impellor intakes liquid aluminum from below and forces mixing with the purge gas. Dissolved hydrogen within the melt diffuses into the gas bubbles, which then

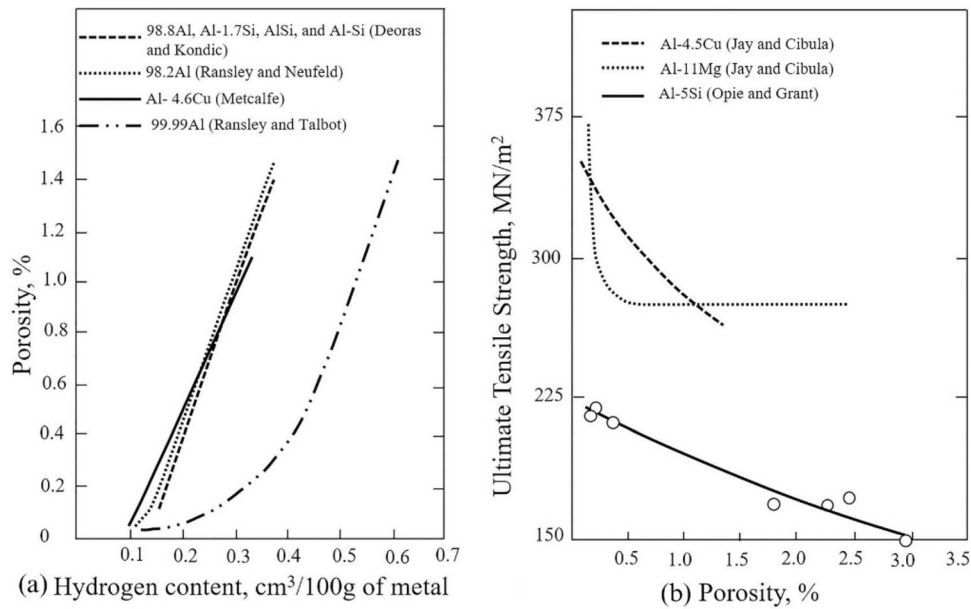


Figure 13. The correlation between hydrogen content and porosity in various aluminum alloys (a) and the correlation between porosity and ultimate tensile strength in various aluminum alloys (b).²⁹

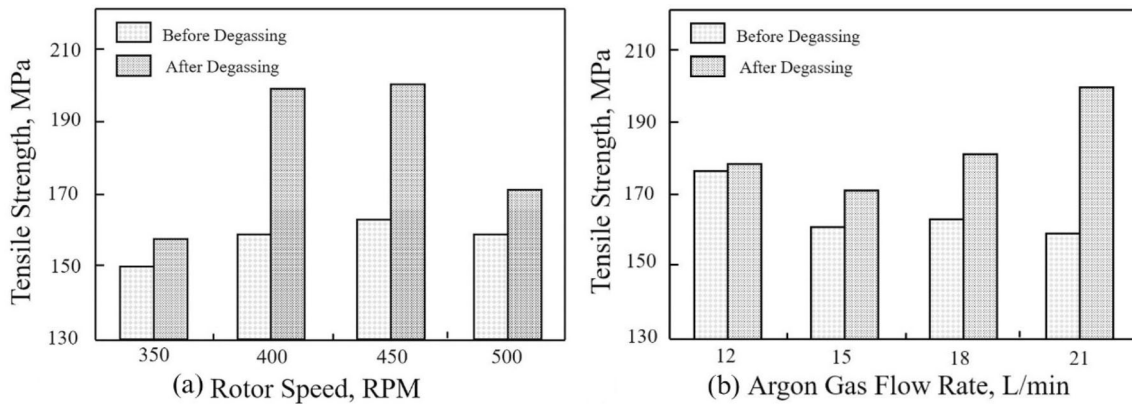


Figure 14. The effect of traditional rotary degassing parameters of (a) rotor speed and (b) argon gas flow rate on tensile strength.³⁶

float upward and carry the diffused hydrogen to the surface. The rotating impellor also breaks up oxides which float upwards to the surface of the melt.^{33,34} Figure 14 shows the benefits of degassing on mechanical properties in an Al-Si-Mg alloy dependent on traditional rotary degassing conditions. Overall, there is an increase in the tensile strength of the alloy when compared to non-degassed samples.

When an ultrasonic wave is applied to a fully liquid melt, cavitation bubbles form as well as full circuit streaming loops. As cavitation bubbles form, hydrogen from within the melt dissolves into the bubbles, which are then swept up by the streaming loops and brought closer to the surface until they reach a minimum depth from which the hydrogen can escape.^{31,35} This is the basis of how UST can degas a

liquid metal. This mechanism is visualized in Figure 15. However, UST can be applied for degassing purposes in various ways: (i) UST fixed frequency without any additional inputs; (ii) UST with variable frequency capability; and (iii) UST fixed frequency in combination with a purge gas.

Recently, Puga et al.,¹⁴ with MPI MMM technology, developed a prototype that allows the combination of mechanical rotation of the system with dynamic ultrasonic agitation. This system increases the efficiency of the metal treatment in cases with large material volumes, low treatment temperatures, or reduced levels of dissolved hydrogen in the medium. Moreover, it has been reported that using UST in MMM modality or in a variable frequency mode

obviates the need to use a purge gas during degassing.¹⁴ (Figure 16)

Figures 17 and 18 show the results of three different degassing methods in terms of hydrogen content and alloy density, respectively. MMM UST degassing and MMM UST degassing with rotation both showed a lower hydrogen content post-processing when compared with traditional argon rotary degassing within the first 2 minutes. MMM UST procedures reach a lower steady state

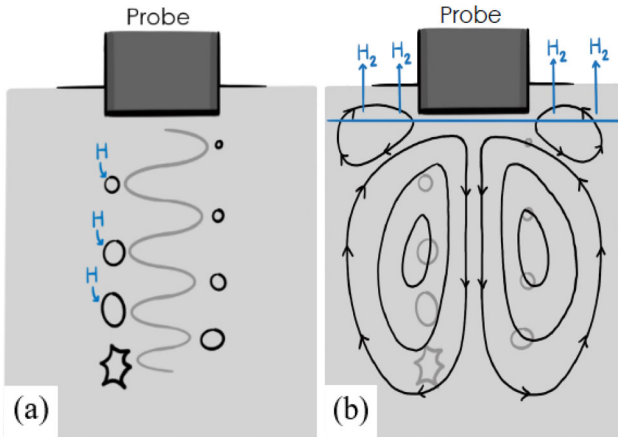


Figure 15. A visual of how UST alone causes degassing of hydrogen via (a) hydrogen dissolving into cavitation bubbles and (b) streaming loop transportation of hydrogen-filled cavitation bubbles.

hydrogen content in less time than traditional rotary degassing, in accordance with MPI data. A reduced pressure test also showed the comparison of traditional with UST degassing for increases in the alloy density with respect to degassing time.¹⁴

UST can also be combined with a purge gas to increase degassing efficiency. Southwire Corp. provides ultrasonic degassing equipment consisting of a ceramic SiAlON solid probe containing three small holes that run through the probe lengthwise. These through-holes allow for the use of a purge gas into the liquid metal in the same direction that the ultrasonic wave is applied into the melt. The basis of this mechanism is that in addition to cavitation bubbles acting as a sink for hydrogen, the purge gas also enhances and complement diffusion of hydrogen to the bubbles. The conceptual framework of this approach is that a combination of cavitation bubbles and purge gas bubbles can interact with more of the melt and thus enhance the efficiency of hydrogen removal. This combination of bubbles is then removed by the streaming loops as discussed above.

Table 1 shows results from a study of UST and purge degassing in a twin-roll casting launder.³⁷ Three conditions were studied. The condition titled “Not optimized” refers to no degassing and thus no efforts were made to lower hydrogen or oxide content. The condition titled “1st Step” refers to methods to reduce turbulence at the surface of the liquid metal to prevent the entrapment of oxides and inclusions. This 1st Step increases hydrogen removal

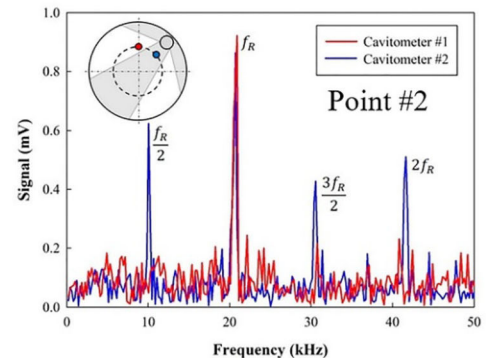
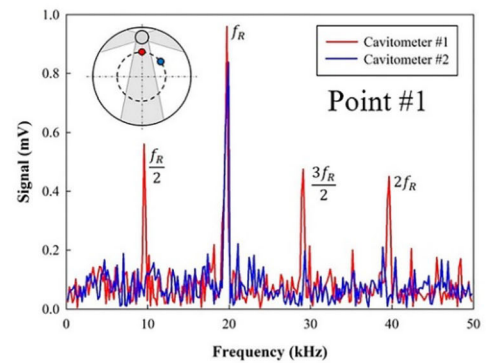
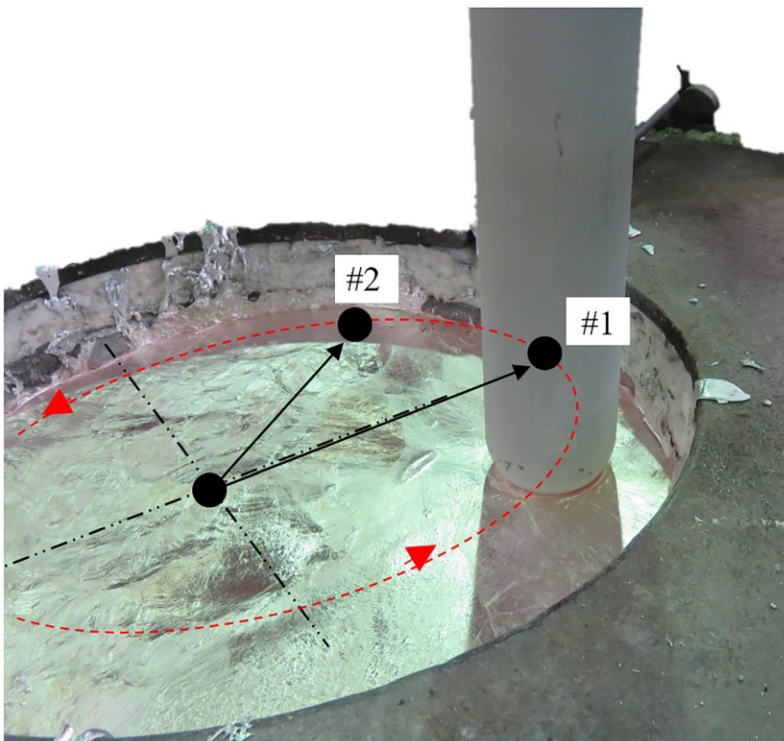


Figure 16. Experimental apparatus for the ultrasonic ceramic sonotrode translation. Level of cavitation registered at Point #1 and #2 - adapted from.¹⁴

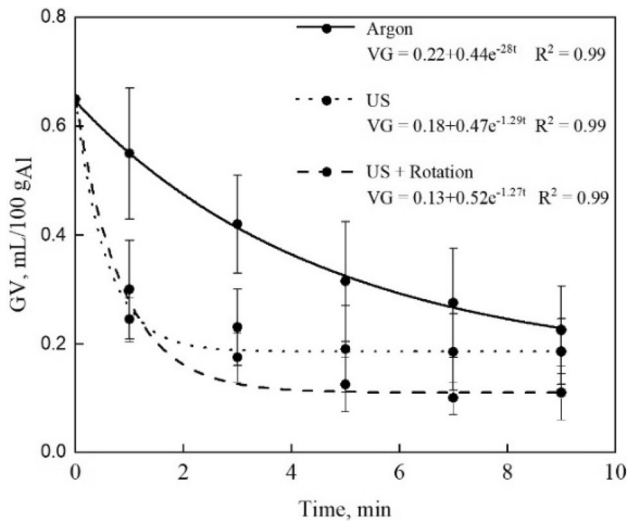


Figure 17. MMM results of hydrogen removal in AISi9-Cu3(Fe) alloy using traditional argon rotary degassing, UST degassing, and MMM UST degassing and with probe rotation.¹⁴

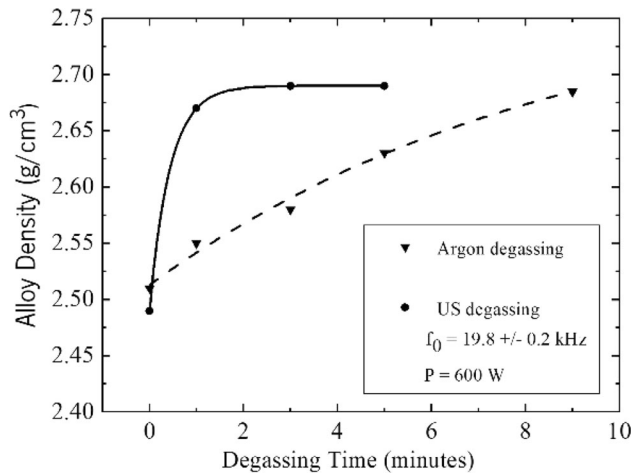


Figure 18. Alloy density vs. degassing time as plotted for MMM UST degassing (solid) and for traditional argon rotary degassing (dashed).¹⁴

efficiency from 45 to 60%. The condition titled “2nd Step” is when purge gas and ultrasonic treatment are carried out together in the launder. The latter increased the removal efficiency from 45 to 77.8%. Figure 19 shows the effect of UST and purge degassing on inclusion and oxide content, which were measured using PoDFA—before and after degassing. Both the oxide films and the various inclusion concentrations were decreased significantly, including the chemical grain refiner.³⁷

Fixed frequency ultrasonic treatment has been studied with respect to multiple system conditions. A study by T. Meek et al investigated the effects of humidity, treatment temperature, and melt volume on the effectiveness and efficiency of UST degassing.³⁸ The experimental setup included a fixed frequency 20kHz ultrasonic generator, a PZT

Table 1. Southwire Results on Degassing That Compare an Unoptimized System As-Cast, to a 1st Step Optimized System, To a 2nd Step Optimized System Involving UST In Combination With A Purge Gas³⁷

Condition	Location	Hydrogen ml/100g	Temperature °C	Removal efficiency (%)
Not optimized	Furnace exit	0.40	760	45.0
	After filter	0.22	706	
1st step	Furnace exit	0.40	760	60.0
	After filter	0.16	707	
2nd step	Furnace exit	0.45	791	77.8
	After filter	0.16	708	

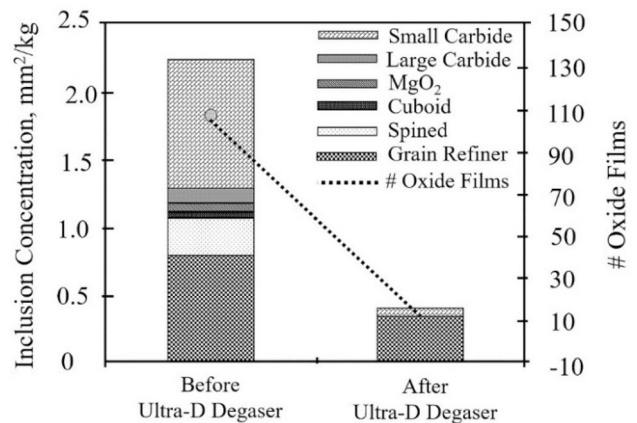


Figure 19. Inclusion concentration before and after degassing with the Southwire degassing system.³⁷

transducer, and a Ti-6Al-4V probe. Their study on humidity evaluated treatment of 0.2 kg of A356 at 740 °C for two different humid environments, 40 % and 60 %. The results recorded hydrogen content using post-cast analysis with respect to UST degassing time, as seen in Figure 20. Their conclusion was that the change in humidity of the environment does not affect the lowest achievable hydrogen content.

Regarding the effect of temperature, Meek et al investigated treatment at four different temperatures for relatively the same humidity. A356 has an approximate liquidus temperature of 615 °C. These trials studies treatment at 620 °C, 660 °C, 700 °C, and 740 °C. The recorded hydrogen content per UST degassing time showed that UST degassing at temperatures closer to the liquidus temperature took significantly longer to reach the lowest steady state hydrogen content, Figure 21. Treatment at

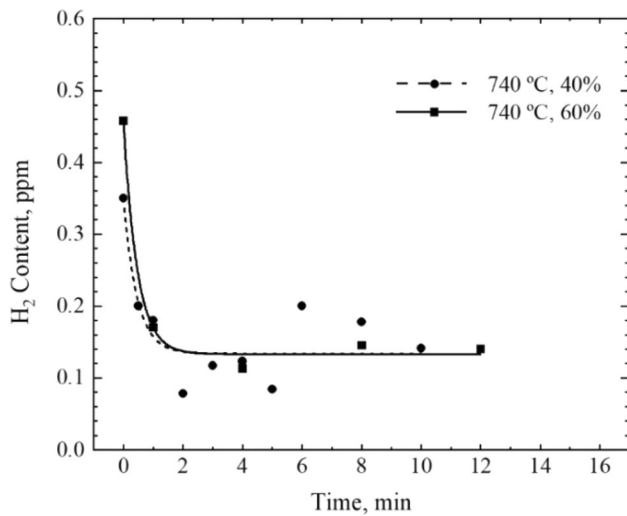


Figure 20. Hydrogen content per UST degassing time in 40 % humidity (dashed) and 60 % humidity (solid).³⁸

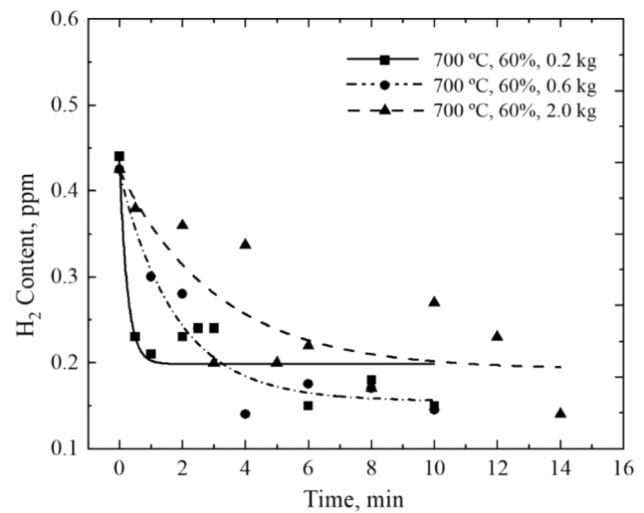


Figure 22. Hydrogen content per UST degassing time in 0.2 kg, 0.6 kg, and 2.0 kg.³⁸

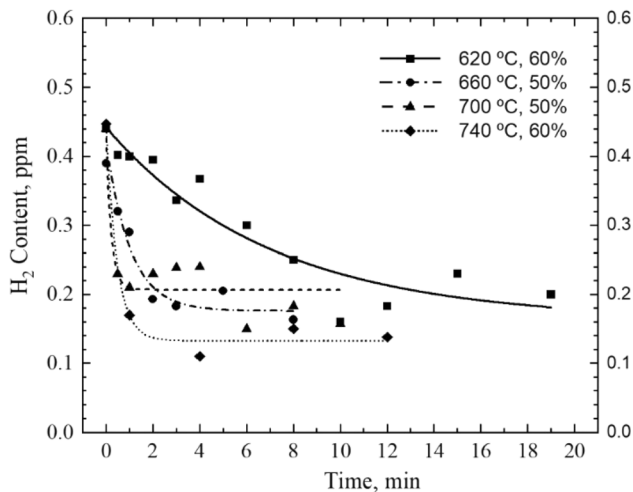


Figure 21. Hydrogen content per UST degassing time at 620 °C, 660 °C, 700 °C, and 740 °C.³⁸

different temperatures did not reach the same lowest steady state hydrogen content. At 620 °C the lowest was not reached during the 20-minute trial. At 660 °C, the lowest steady state hydrogen content took approximately 3 minutes to reach and was lower than what was achieved at 700 °C which reached the lowest steady state hydrogen content within approximately 1.5 minutes. At 740 °C the steady state hydrogen content was the lowest of all the trials and was reached in approximately 1.5 minutes.³⁸ These data contradict what is observed in traditional rotary degassing. Traditional rotary degassing is most efficient at lower temperatures because the influx of hydrogen at the surface is minimized with lower temperatures. The data in Figure 21 show the opposite, that for UST degassing a higher temperature is favored. This can be explained via the viscosity of the metal being treated. As the temperature drops, the viscosity of molten metal increases. When the viscosity is raised, ultrasonic energy is dampened and

absorbed sooner than in a lower viscosity melt, thus reducing the effective treatment.

The study on different volumes of melt investigated UST degassing of a 0.2 kg, 0.6 kg, and 2.0 kg melt. All trials were treated at 700 °C and 60 % humidity. As the size of the melt increased, the time required for UST degassing increased, as expected. Figure 22 depicts how the melts reach a relatively similar steady state hydrogen content. A 0.2 kg melt reached steady state within 2 minutes, while a 2.0 kg melt reaches steady state after 6 minutes. The conclusion made was that regardless of melt size, a similar steady state hydrogen content is possible with different UST degassing times.³⁸

Meek's study claims that UST degassing with a purge gas significantly decreases the amount of dross formation.³⁸ UST purge degassing functions through the introduction of a purge gas during UST. The presence of a purge gas is suspected to increase the survival and presence of bubbles that ultrasonic energy can act on in the melt. Table 2 shows the amount in grams of dross produced via traditional argon degassing and UST purge degassing for a specified degassing time for a 5.0 kg melt of A356. At every time there is significantly less dross produced with UST purge degassing than there is for traditional rotary degassing.

A recommendation for future research is to study the formation of a cavitation bubble and determine the composition inside the bubble, which is a difficult task. It is commonly believed that cavitation bubbles form around weak points in the melt such as hydrogen that is adsorbed to the surface of an oxide or inclusion or that the bubbles fill with aluminum vapor during the stages of cavitation.⁶ For the first reason to be the case, there would have to be a minimum hydrogen content for cavitation bubbles to form in molten aluminum. This is a path of study that should be

pursued to mechanistically define cavitation and develop an optimum process for UST degassing. UST purge degassing should be compared with UST degassing alone in terms of dross production and lowest possible steady state hydrogen content.

Intermetallic Morphology Modification

The presence of deleterious intermetallic compounds reduces the mechanical properties of the cast product. Intermetallic phase morphology, i.e., size and shape, is influenced by the composition as well as processing conditions. The 3XX series Al alloys are a good example, wherein harmful intermetallic compounds form due to the presence of both silicon and iron. The β -phase, or Al_5FeSi , forms early-on during solidification and with a large enough iron content, this phase experiences unrestricted growth. The β -phase forms in a platelet morphology, which on a 2D micrograph can be observed as needles.³⁹ The Al_5FeSi needles are hard, brittle, and serve as crack-initiation sites.^{40,41} The α -phase, or the Al_8Fe_2Si phase, forms

before the β -phase and has a unique ‘crinkled’ shaped. This phase causes less harm on mechanical properties than the β -phase, however it is still an undesirable phase. Figure 23 shows the size and shape of the β -phase as well as the α -phase in an Al-Si-Fe alloy.

In terms of modifying the morphology of these intermetallic compounds, there are few procedures to regulate their growth. A common technique for Al-Si-Fe alloy systems where the iron content is 0.45 wt% iron or more is to maintain a minimum 2:1 ratio of iron to manganese in the alloy.^{36,42} The manganese presence in this ratio restricts the formation of the β -phase by producing more of the α -phase first and exhausting more iron in this formation.⁴³ This method lowers the amount of β -phase and improves mechanical properties minimally as the presence of the α -phase is still detrimental to mechanical properties. The consequence of this technique is that the addition of manganese increases the amount of slag production. Cooling rate provides another method of regulating the size and morphology of these iron-based intermetallics. A fast-cooling rate restricts the total size that the intermetallic can grow to since the intermetallics are the first phases to solidify.⁴⁴ Intermetallic growth can be controlled effectively by synchronizing the cooling rate and manganese content of Al-Si-Fe alloys, as seen in Fig. 24. In general, a higher cooling rate and moderate manganese content produce a less harmful β -phase morphology. Although this is an effective method of regulating intermetallic growth, it is unfortunately a new restriction both compositionally and process-wise.

Techniques for intermetallic modification are effective, however, they exhibit restrictions on the composition and/or processing method of the cast-part. The use of UST to modify intermetallic morphology is a recent development which is being actively investigated at the ACRC. The concept is based on the capability of intermetallic phase morphology to be altered by shearing forces and the ability

Table 2. Amount of Dross Production in Grams for Traditional Degassing and UST Purge Degassing With Respect to Degassing Time³⁸

Degassing method	Degassing time (min)						
	2	5	10	15	20	25	
Argon degassing alone	NA	16.6		22.8 ^a	39.4	49.5	65.1
Argon degassing with ultrasonics	0.9		1.8 ^a	5.2	6.4	NA	NA

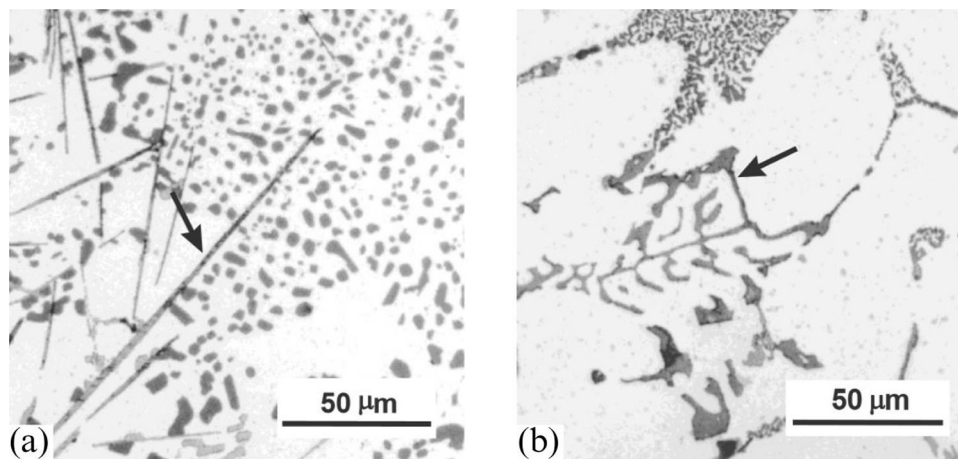


Figure 23. Micrographs of an Al-5Si-1Cu-0.5Mg-(Fe) alloy showing (a) the β -phase and (b) the α -phase.³⁹

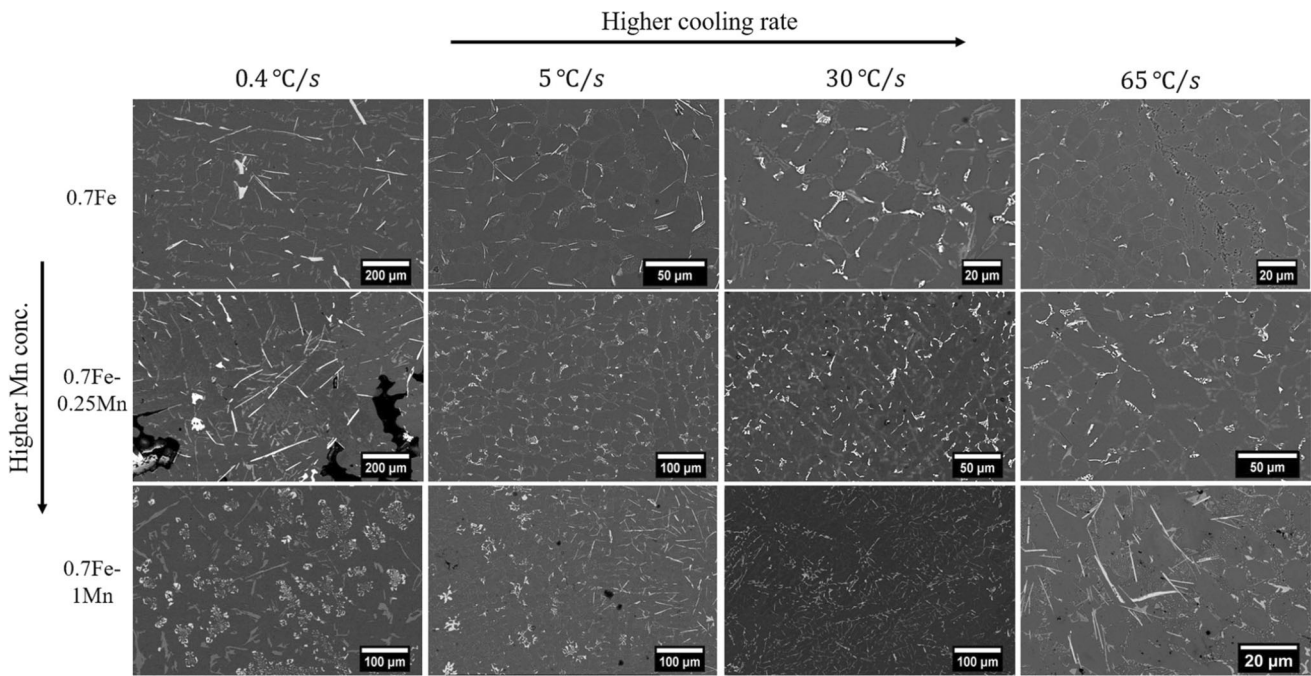


Figure 24. An array of microstructural changes in the Al-8Si-0.35Mg-0.7Fe alloy with both increases in cooling rate and increases in manganese concentration from the top left to bottom right.⁴⁴

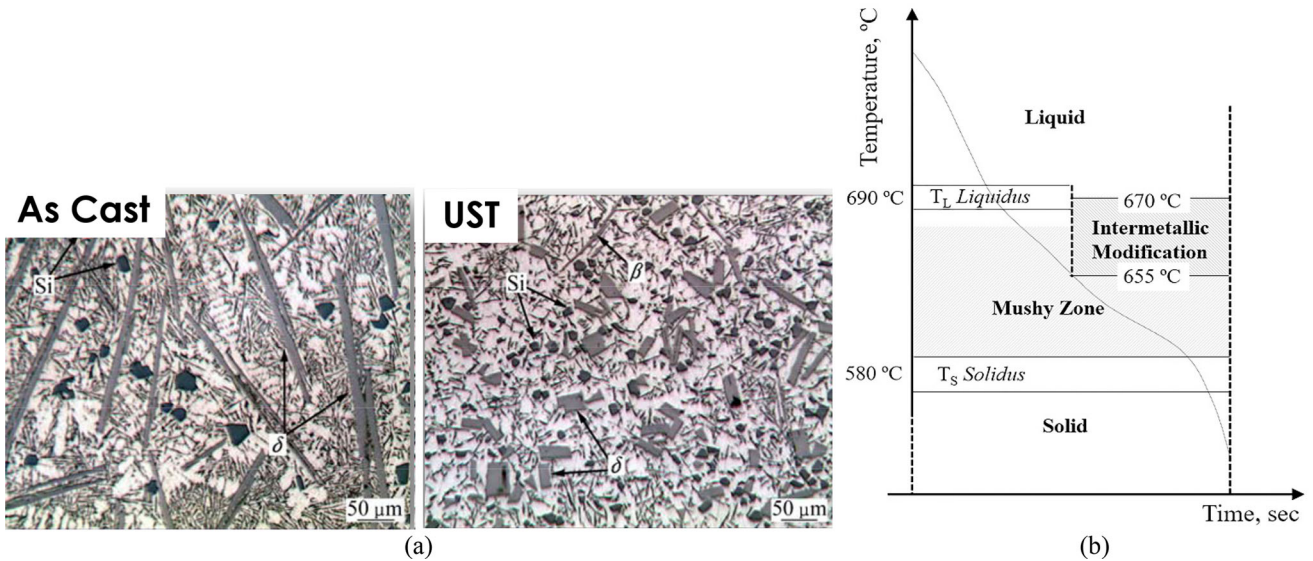


Figure 25. (a) Al-17Si-4Fe samples without and with ultrasonic treatment⁴⁰ (b) a visual representation of the UST application temperature range.

of ultrasonic waves to exhibit shearing action in a liquid or slurry (Figure 25).

The method by which ultrasonic waves refine the morphology of intermetallics can vary dependent on the temperature of treatment. Intermetallic phases in molten aluminum such as the β -Al₃Fe Si or α -Al₈Fe₂Si form at the forefront of solidification in the system. Traditionally, literature has shown ultrasonic treatment to be applied below the liquidus temperature, after the primary intermetallic

phases have begun to solidify. In this method of intermetallic modification via UST, both acoustic streams and acoustic cavitation work together to fragment the formed intermetallic phases. Figure 25 shows the effect of UST on a hypereutectic Al-Si-Fe alloy. The intermetallics in the UST sample are simply the fragmented and broken-up versions of the intermetallics seen in the as-cast sample. This Al-17Si-4Fe alloy has an expected liquidus temperature of 690 °C and treatment was applied below that during

the fully mushy zone starting from 675 °C and ending at 655 °C before the solidus temperature of 580 °C.⁴⁰

A study on hypereutectic Al-19Si-4Fe alloy by C.J. Todaro et al.,¹³ investigated the formation of intermetallic phases with and without ultrasonic treatment.¹³ Todaro carried out UST treatment at 690 °C which is above the liquidus temperature of 665 °C and ended the treatment at 610 °C. Figure 26 displays the microstructural change from the as-cast to the UST treated sample. To explain the effect of UST on the intermetallic formation, it is useful to compare this microstructural change to that of Figure 25 where the Al-17Si-4Fe alloy was treated below the liquidus temperature. This implies that the intermetallic phases formed were subsequently broken up by the applied ultrasonic energy. This is visible in Figure 25 where the as-cast samples have long, sharp, plate-like phases and the UST sample has small chunks. This can be explained by the mechanism of phase fragmentation. When the temperature dropped below the liquidus, the intermetallic phase formation commenced. As UST was applied, these long intermetallic phases were fragmented into smaller pieces.

However, the microstructural change in Figure 26 cannot be explained by the mechanism described above. Instead of smaller pieces that were clearly fragmented - Figure 25, the UST sample in Figure 26 shows that the intermetallics were not fragmented but underwent a different formation mechanism. Todaro et al.,¹³ explains this via the peritectic transformation of the δ -Al₃FeSi₂ into β -Al₅FeSi. In the as-cast alloy, the intermetallic plate-like phases are the β -Al₅FeSi that envelope the δ -Al₃FeSi₂.¹³ This means that the peritectic transformation did not go to completion as expected in Figure 29.

UST-assisted peritectic transformation may also cause changes in the formation of different intermetallic phases in Al-Si-Fe alloy systems. For example, the A380 alloy contains up to 1.3 wt% iron and has an approximate liquidus temperature of 593 °C and a solidus temperature of 538 °C. Figure 29 shows the Scheil solidification profile for Al alloy with Si 8 wt%, Fe 1.3 wt%, Mn 0.5 wt%, Cu 0.2 wt%, Mg 0.4 wt%, Zn 0.1 wt%, and Ti 0.2 wt%. The “Al₉Fe₂Si” phase is the β -Al₅FeSi and is calculated to be the first phase to solidify. The high iron content is responsible for the immediate and long formation of the detrimental β -Al₅FeSi. When ultrasonic treatment is applied in the melt, acoustic streaming occurs and as the melt approaches the liquidus temperature, compositional diffusion induces the precipitation of iron-based intermetallic compounds. However, the introduction of ultrasonic energy disrupts this diffusion via acoustic streaming. This streaming alters both the size and morphology of the intermetallic compounds forming within the melt. Acoustic streaming causes the melt composition to homogenize and therefore less of the required composition is available in one location to form these intermetallics. This decrease in available composition results in the intermetallic compounds such as the β -phase being smaller and more closely dispersed rather than larger and farther apart. Similarly, as ultrasonics continue to be applied to the melt from before to after intermetallic phase formation, the compositional diffusion that occurs during phase formation is assisted and altered which affects the resultant morphology.

A study by Zhao *et al.* provides further results and theories for intermetallic fragmentation in an Al-Cu alloy.⁴⁵ Al-5.0Cu-0.6Mn-0.5Fe and -1.0 Fe alloys were treated with ultrasonics through solidification, starting above the liquidus and ending about 100 °C below the liquidus. X-ray

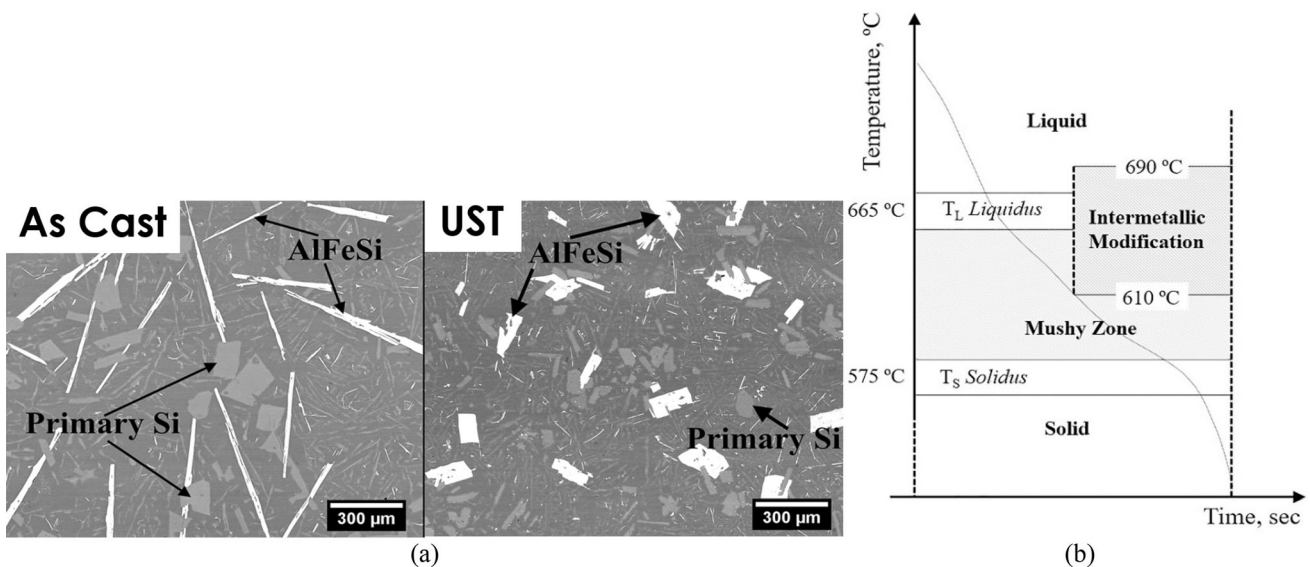


Figure 26. (a) Al-19Si-4Fe without and with ultrasonic treatment¹³ (b) a visual representation of the UST temperature range.

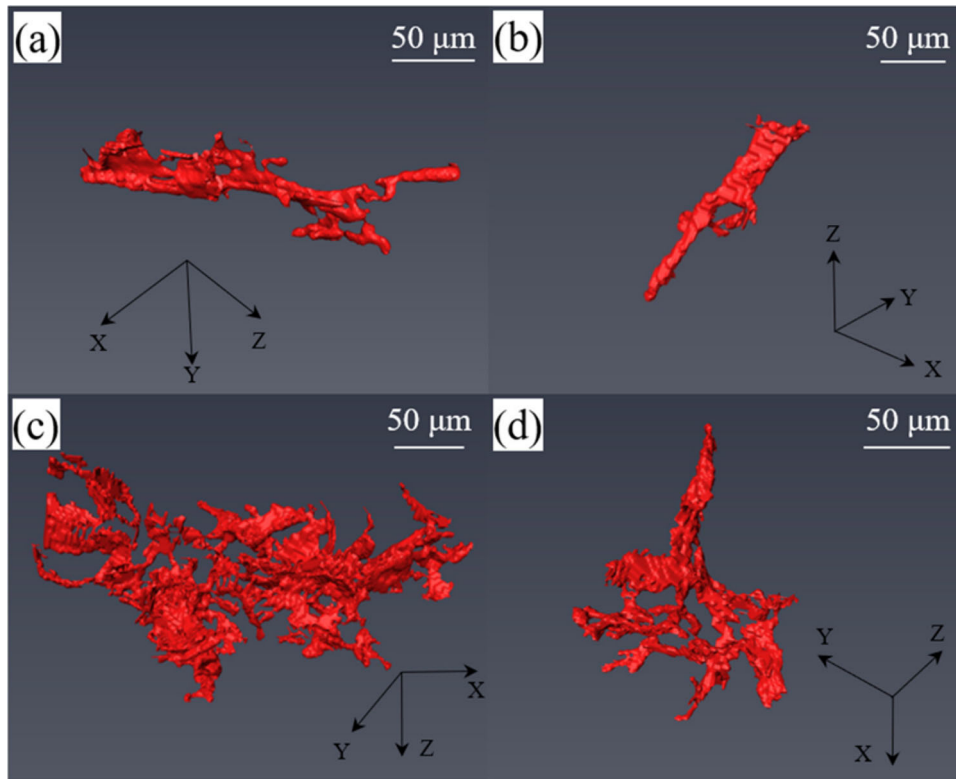


Figure 27. (a, c) Untreated intermetallic phases $\text{Al}_3(\text{FeMn})$ and $\alpha - \text{Al}_{15}(\text{FeMn})_3\text{Cu}_2$, respectively, (b, d) their UST counterparts.⁴⁵

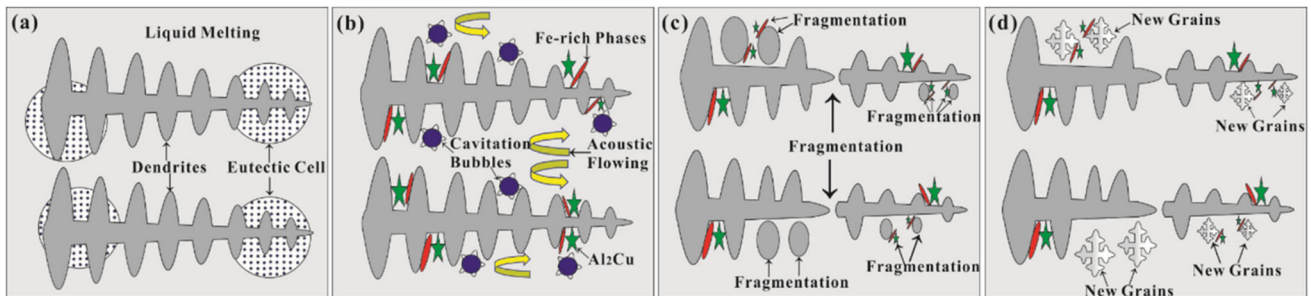


Figure 28. A visualization of the mechanisms, dendritic and intermetallic fragmentation.⁴⁵

synchrotron tomography results show the 3D rendering of the intermetallic phases $\text{Al}_3(\text{FeMn})$ and $\alpha - \text{Al}_{15}(\text{FeMn})_3\text{Cu}_2$ (Figure 27). After UST, the average intermetallic network is reduced in size and complexity, with less branching networks overall. The major conclusion was that in the same way dendrites can be fragmented by cavitation bubbles, intermetallic phases also experience the same fragmentation with treatment that proceeds through the first stages of solidification, presented visually in Figure 28.

Future studies for the intermetallic morphology modification via ultrasonic energy should aim to define parameters necessary to affect the formation of these intermetallic phases. A study on the required temperature treatment

range would further explain the mechanisms that occur to affect intermetallic formation.

Grain Refinement

Grain refinement is traditionally achieved via the addition of grain refiners such as titanium boride to the molten metal.⁴⁶ Grain refining rod master alloys made of Al-5Ti-B are commonly added to A365 in 0.5 wt%.⁴⁷ Grain refiner particles act as nuclei for heterogenous nucleation.⁴⁸ (Figure 29)

Ultrasonic treatment can grain refine the melt without the addition of external agents.⁴⁹ The bubble collapse that results from acoustic cavitation exerts force on solidifying

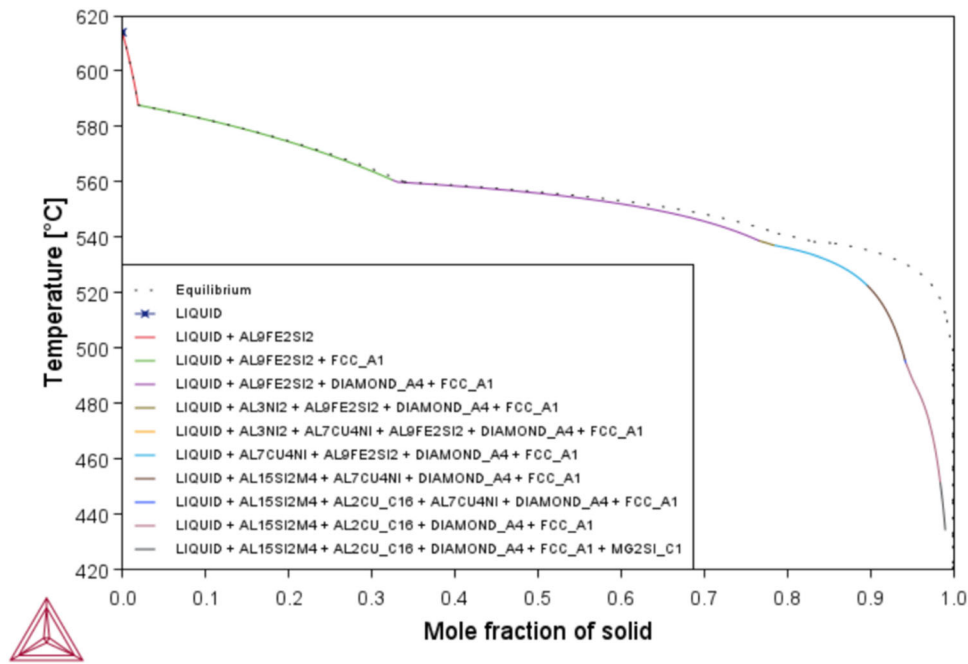


Figure 29. A Scheil solidification curve of an example A380 composition.

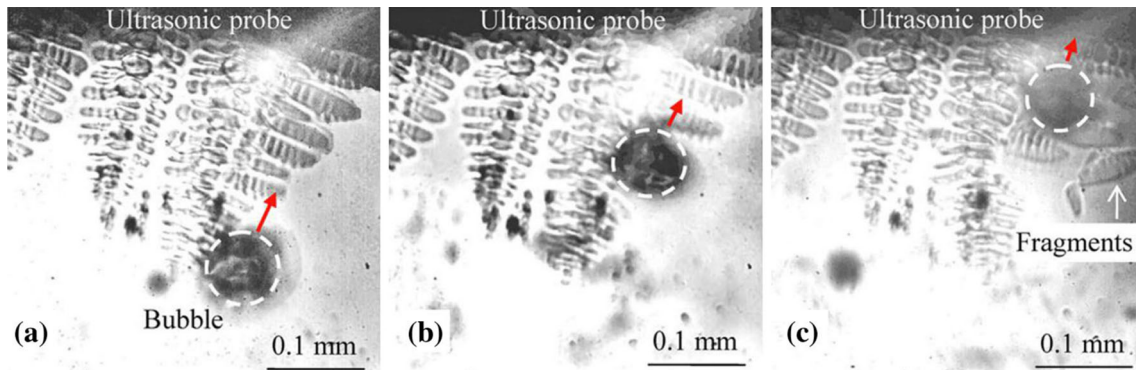


Figure 30. The procession of a suspected cavitation bubble fragmenting dendrites in a semi-solid melt.⁵⁰

interfaces which leads to fragmentation of oxides at high temperatures and dendrites at low temperatures.^{13,26,50,51} Figure 30 shows in situ x-ray radiography imaging of a cavitation bubble fragmenting dendrites in a semi-solid melt.⁵⁰ The high velocity streams that follow cavitation bubble collapse also exert forces on solidifying dendrites leading to fragmentation.⁵² These dendrite fragments are further broken down by these two mechanisms and are carried by acoustic streaming around the melt volume. As solidification continues, these fragments act as nucleation sites for heterogenous nucleation, resulting in a fine and globular structure.⁶ Ultrasonic treatment is an effective in situ grain refiner without the addition of external agents.

Figure 31 shows the effect of ultrasonic treatment and the resultant refined the microstructure of A356 treated at 670 °C.⁵³ In the same work, it was found that the constituents of the eutectic phase were modified subsequent to

ultrasonic treatment, Figure 32. Table 3 displays the mechanical properties of brass samples produced via different refining processes. The mechanical behavior of the cast brass shows an increase through chemical refinement and similarly there is an increase through ultrasonic treatment.⁵⁴

UST grain refinement works most efficiently at lower temperatures, below the liquidus. Figure 33 shows the effect of grain refinement when UST is applied in the liquid state at 700 °C. There is some evidence of refinement, however, the refinement is not as apparent as when treatment is applied in the liquid-solid state, as seen in Figure 31.⁵³ When ultrasonic treatment is stopped before the onset of solidification, dendrites can form without any impact of streams and cavitation.

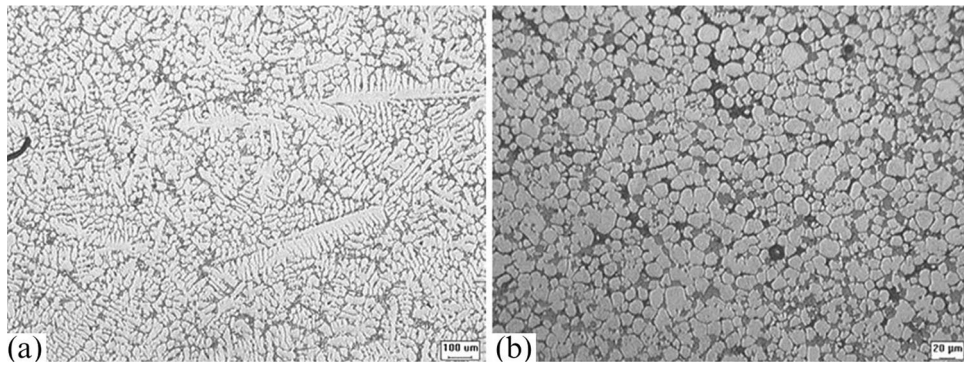


Figure 31. The microstructure of untreated A356 (a) and the microstructure of UST grain refined A356 (b).⁵³

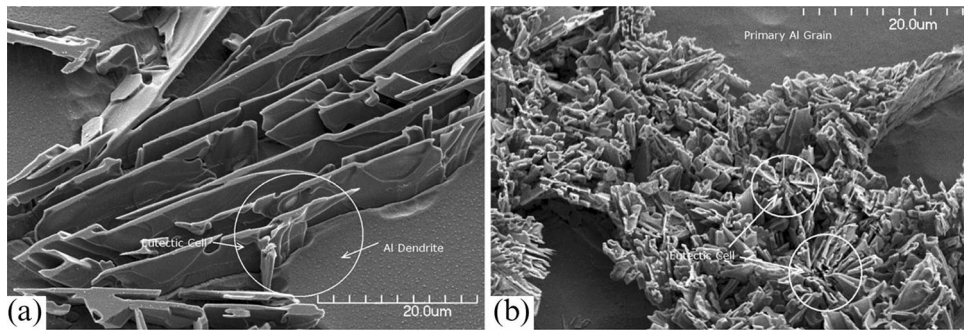


Figure 32. The eutectic structure of untreated A356 (a) and the eutectic structure of UST grain refined A356 (b).⁵³

Table 3. UTS, Yield Stress, and Elongation Values of Brass Samples Produced Via Different Refining Techniques⁵⁴

Refinement technique	UTS (MPa)	Yield stress (MPa)	Elongation (%)
Not refined	282 (± 30)	178 (± 14)	4.3 (± 1.0)
Chemical refinement	310 (± 15)	181 (± 11)	5.0 (± 0.7)
Ultrasonic refinement at 900 °C	345 (± 15)	183 (± 10)	6.9 (± 0.5)
Ultrasonic refinement at 920 °C	367 (± 12)	187 (± 7)	9.4 (± 0.6)
Ultrasonic refinement at 940 °C	386 (± 10)	192 (± 7)	11.5 (± 0.6)

There has been evidence of grain refinement that results from ultrasonic treatment during the liquid state with some superheat, when there is no solid fraction. Liquid state grain refinement has been accomplished in A356 treated above the liquidus temperature (615 °C) with multifrequency ultrasonics applied at 680 °C.¹⁶ Figure 34 shows the evident grain refinement from dendritic to globular as well as refinement in the eutectic phase. This treatment temperature is lower than the previous study which treated A356 at 700 °C. The potency of grain refinement via UST is strengthened with lower treatment temperatures.

A branch of UST research involves the combination of ultrasonics with a secondary processing method that may enhance the potency of treatment.^{55–57} One study by Zhao *et al.* investigates the combination of UST with applied

pressure (AP). An Al-5Cu-0.6Mn-0.5Fe-0.6Si recycled alloy composition was treated with 20 kHz UST and poured at various temperatures with an applied pressure of 50 MPa.⁵⁵ The results showed that treatment (UST and AP) and pouring at a higher temperature brought finer grain refinement. Figure 35 shows the change in grain refinement with different pouring temperatures. This disagrees with the previous statement that UST grain refinement is more potent at lower temperatures. This study places the perspective on the effect of UST and AP on the cooling rate. The study compared the cooling curve of a gravity cast to a UST and AP sample both poured at 710 °C, Figure 36. UST and AP greatly increased the cooling rate which is a known method of inducing grain refinement.⁵⁸ A concern that should be acknowledged within this research is the use of a titanium ultrasonic probe. As mentioned in the section

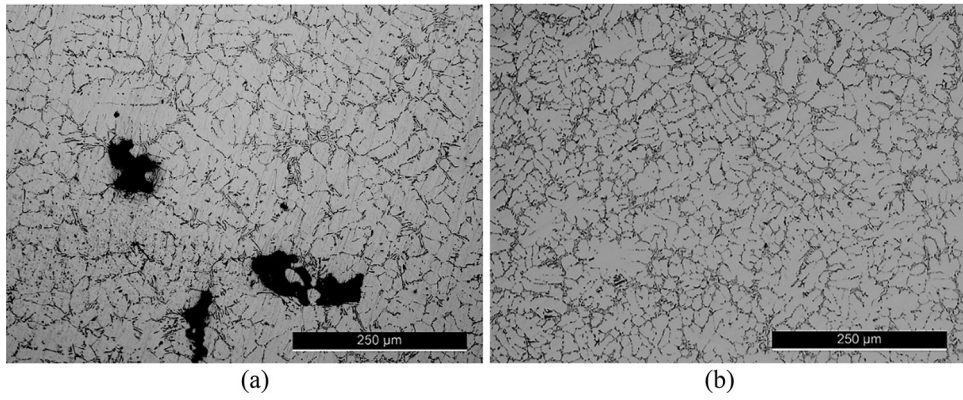


Figure 33. A microstructure of A356 untreated (a) and treated with UST in the liquid-state (b).

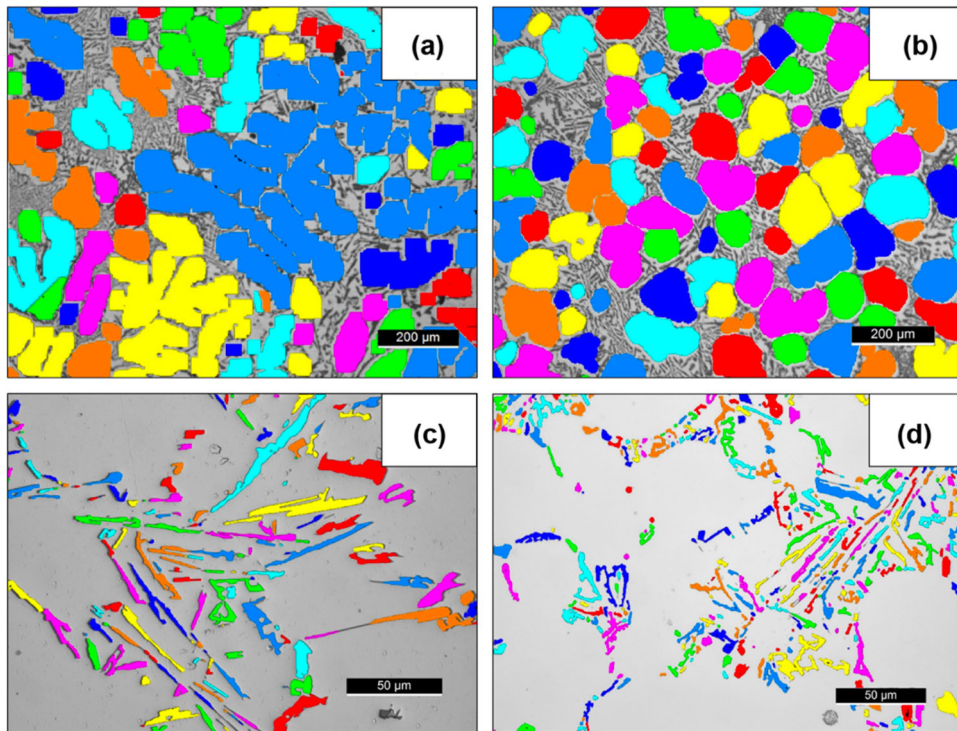


Figure 34. (a, c) Untreated A356 (b, d) UST grain and eutectic refinement from liquid state treatment.¹⁶

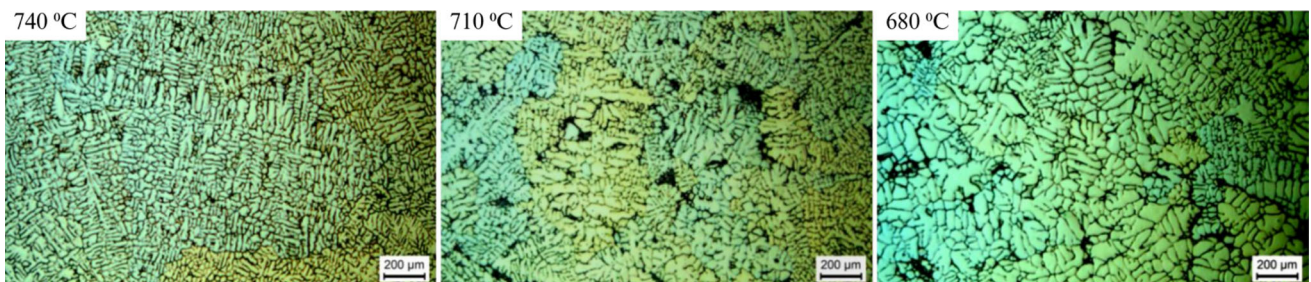


Figure 35. Change in grain refinement effects as a result of pouring temperature in a cast processed via UST and AP.⁵⁵

on ultrasonic instrumentation, titanium probes are much more likely to erode into the melt and introduce titanium contamination which may benefit the grain refining results.

A study by Wang et al suggests that any grain refinement that results from ultrasonic treatment during the liquid state is attributed to the fragmentation of oxides.¹² During liquid state treatment, there are no solid interfaces on which

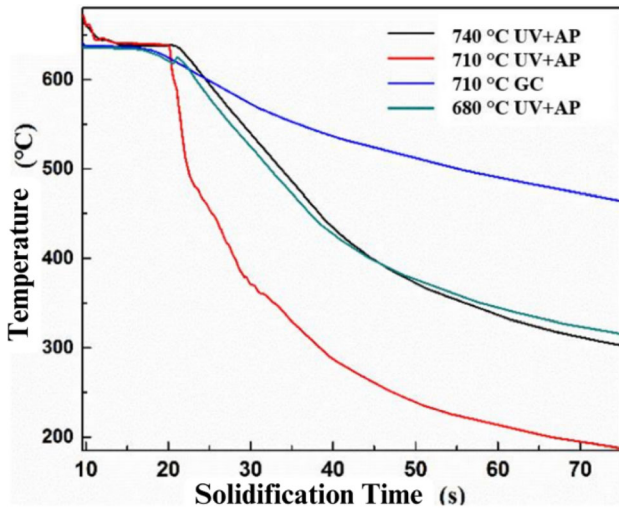


Figure 36. Cooling curves with respect to pouring temperature and process.⁵⁵

cavitation and streaming can act on, however, Al_2O_3 oxides are present, which are fragmented and act as in-situ grain refiners. In Al-0.4Ti wt% alloy, the primary intermetallic that forms are Al_3Ti . It was found that Al_3Ti intermetallics nucleate around Al_2O_3 oxide particles. Upon the application of UST in the liquid state from 810 to 770 °C, the oxide clusters in the melt were broken up and homogeneously dispersed via acoustic cavitation and streaming. Al_3Ti intermetallic forms around the oxide nuclei. Cavitation and streaming continue to fragment the plate-like structures, seen in (Figures 37 and 38)¹². Figure 38 shows the oxide particles found at the center of refined intermetallic compounds.¹² The evidence that broken down oxide clusters may act as internal grain refiners through liquid state UST now leads to the question, what is the minimum or maximum content of oxides that must be present for this mechanism to be successful?

Summary

Ultrasonic energy imparted into the molten metal has the capability to affect and modify the resultant cast structure. While ultrasonic energy applications for liquid metallurgical processes have stable roots at the laboratory level, they are still in their early stages when it comes to industrial-scale implementation. Applications vary from distributing second phase nanoparticles in the melt, to

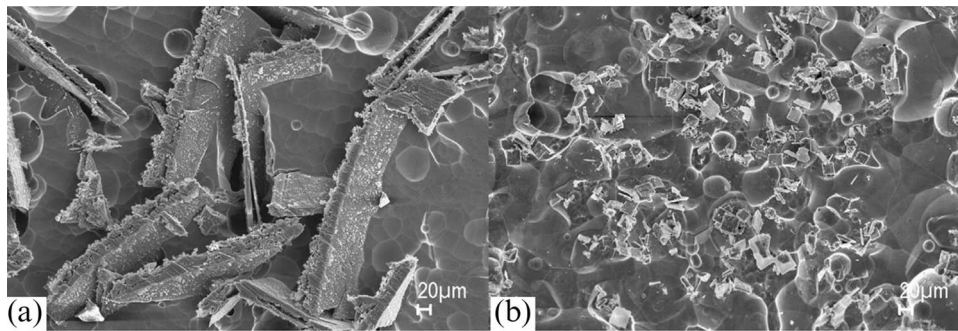


Figure 37. Al_3Ti particles without UST (a) and with UST (b).¹²

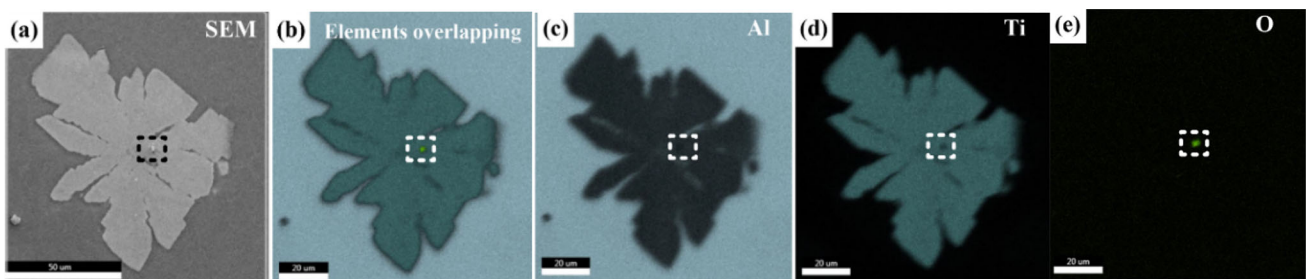


Figure 38. Characteristics of an oxide particle in the center of an Al_3Ti particle refined by UST: (a) SEM image; (b) overlapped EDS mapping image of Al, Ti and O elemental distributions; (c) EDS mapping of Al elemental distribution; (d) EDS mapping of Ti elemental distribution; (e) EDS mapping of O elemental distribution.¹²

breaking up the oxides and causing in-situ grain refinement, to modifying the intermetallics that form during the early stages of solidification.

There are three types of ultrasonic energy delivery; (i) fixed-frequency UST, (ii) fixed-frequency UST in combination with a purge gas, and (iii) variable frequency UST. Fixed-frequency UST is the most common form of treatment in literature. The goal of the combination of a fixed-frequency UST with a purge gas is to increase the survival and existence of cavitation bubbles to increase the effectiveness of treatment. Multifrequency UST focuses on system resonance to increase the effectiveness of treatment. The choice of treatment temperature is crucial to take advantage of ultrasonic mechanisms for targeted applications.

In UST degassing, the treatment temperature should be high enough that the viscosity of the liquid metal allows for undampened treatment. In UST intermetallic morphology modification, the treatment mechanism changes with temperature from either fragmentation at a temperature where the intermetallics have already formed, or UST-assisted diffusion at a temperature where the intermetallics are about to form. Similarly in grain refinement, the mechanisms are dependent on temperature where fragmentation rules at a temperature below the liquidus.

In this work, we have reviewed the various ultrasonic delivery methods, and their effects on the resultant microstructural characteristics of the cast product. Specifically, processing parameters such as temperature, ultrasonic density per volume, and the interaction of the probe with the melt are fertile domains for further work.

Acknowledgements

The authors gratefully acknowledge funding from the Advanced Casting Research Center (ACRC). The authors acknowledge strategic partnerships with AMETEK, Buehler, and Evident Scientific, VJT. Special thanks to EMC for hydrogen analyses, and MPI Ultrasonics for their assistance regarding Multifrequency, Multimode, Modulated Sonic & Ultrasonic Vibrations technology.

Conflict of interest The authors declare that they have no known competing interests, financial, or personal relationships that could influence the work of this paper.

Open Access This article is licensed under a Creative Commons Attribution 4.0 International License, which permits use, sharing, adaptation, distribution and reproduction in any medium or format, as long as you give appropriate credit to the original author(s) and the source, provide a link to the Creative Commons licence, and indicate if changes were made. The images or other third party material in this article are included in the article's Creative Commons licence, unless indicated otherwise in a credit line to the material. If material is not

included in the article's Creative Commons licence and your intended use is not permitted by statutory regulation or exceeds the permitted use, you will need to obtain permission directly from the copyright holder. To view a copy of this licence, visit <http://creativecommons.org/licenses/by/4.0/>.

REFERENCES

1. S. Singh, P. Ansari, C. Verma, J. Menghani, Effect of grain refinement, modifier and stirring on properties of A356. *Mater. Today Proc.* **4**(2), 734–739 (2017). <https://doi.org/10.1016/j.matpr.2017.01.079>
2. Y. S. Han, “Effect of intermetallic phases on the mechanical properties of cast A356 alloy wheels,” *2006 International Forum on Strategic Technology*, 2006. doi: <https://doi.org/10.1109/IFOST.2006.312324>.
3. C.H. Cáceres, B.I. Selling, Casting defects and the tensile properties of an AlSiMg alloy. *Mater. Sci. Eng. A* **220**(1), 109–116 (1996). [https://doi.org/10.1016/S0921-5093\(96\)10433-0](https://doi.org/10.1016/S0921-5093(96)10433-0)
4. Y.W. Shao, Y. Liu, J.F. Leng, K. Zhu, Z.M. Liu, C.X. Li, Microstructure of as-cast 7085 aluminum alloy by homogenization. *Mater. Sci. Forum* **898**, 265–271 (2017). <https://doi.org/10.4028/www.scientific.net/MSF.898.265>
5. M. Wang, W. Xu, Q. Han, Study of refinement and morphology change of AlFeSi phase in A380 alloy due to addition of Ca, Sr/ Ca, Mn and Mn, Sr. *Mater. Trans.* **57**, 1509–1513 (2016). <https://doi.org/10.2320/matertrans.M2015329>
6. G.I. Eskin, D.G. Eskin, *Ultrasonic Treatment of Light Alloy Melts*, 2nd edn. (CRC Press, 2014). <https://doi.org/10.1201/b17270>
7. S. Wang, J. Kang, X. Zhang, Z. Guo, A study on the effect of ultrasonic treatment on the microstructure of Sn-30 wt% Bi alloy. *Materials* **11**(10), 1870 (2018). <https://doi.org/10.3390/ma11101870>
8. X. Liu, S. Jia, L. Nastac, Ultrasonic cavitation-assisted molten metal processing of cast A356-nanocomposites. *Int. J. Met.* **8**(3), 51–58 (2014). <https://doi.org/10.1007/BF03355591>
9. “Acoustic impedance and reflected energy in ultrasonics.” Accessed: Nov. 11, 2022. [Online]. Available: <https://www.linkedin.com/pulse/acoustic-impedance-reflectivity-ultrasonics-fernando-villa-nueva>
10. G. Sha, C.J. Lissenden, Modeling magnetostrictive transducers for structural health monitoring: ultrasonic guided wave generation and reception. *Sensors* **21**(23), 7971 (2021). <https://doi.org/10.3390/s21237971>
11. M. Redwood, Transient performance of a piezoelectric transducer. *J. Acoust. Soc. Am.* **33**(4), 527–536 (1961). <https://doi.org/10.1121/1.1908709>
12. F. Wang, D. Eskin, J. Mi, T. Connolley, J. Lindsay, M. Mounib, A refining mechanism of primary Al₃Ti intermetallic particles by ultrasonic treatment in the

- liquid state. *Acta Mater.* **116**, 354–363 (2016). <https://doi.org/10.1016/j.actamat.2016.06.056>
13. C.J. Todaro, M.A. Easton, D. Qiu, G. Wang, D.H. StJohn, M. Qian, The effect of ultrasonic melt treatment on macro-segregation and peritectic transformation in an Al-19Si-4Fe alloy. *Metall. Mater. Trans. A* **48**(11), 5579–5590 (2017). <https://doi.org/10.1007/s11661-017-4325-1>
 14. H. Puga, J. Barbosa, V.H. Carneiro, F.V. Barbosa, J.C. Teixeira, Optimizing high-volume ultrasonic melt degassing using synchronized kinematic translation. *J. Mater. Res. Technol.* **14**, 2832–2844 (2021). <https://doi.org/10.1016/j.jmrt.2021.08.098>
 15. “13—Power ultrasonics for additive manufacturing and consolidating of materials | Elsevier Enhanced Reader.” Accessed: Nov. 13, 2022. [Online]. Available: <https://reader.elsevier.com/reader/sd/pii/B9781782420286000132?token=C8B47DD7F27B7E2F188291FD377755F56468773C624C5A3D7462CD8C235100081F28F0A499A679C9E6BB6022C65074BA&originRegion=us-east-1&originCreation=20221113204711>
 16. H. Puga, S.D. Tohidi, V.H. Carneiro, J. Meireles, M. Prokic, Ceramic sonotrodes for light alloy melt treatment. *Int. J. Met.* **15**(2), 459–469 (2021). <https://doi.org/10.1007/s40962-020-00476-5>
 17. “What are Sialon Ceramics?,” International syalons. Accessed: Nov. 12, 2022. [Online]. Available: <https://www.syalons.com/resources/articles-and-guides/sialons/>
 18. H. Feng, G.V. Barbosa-Cánovas, J. Weiss (eds.), *Ultrasonic Technologies for Food and Bioprocessing* (Springer, New York, 2011)
 19. “Southwire.” Accessed: Nov. 25, 2022. [Online]. Available: <https://www.southwire.com/newsroom/archive/scr-develops-state-of-the-art-ultrasonic-dtm-degasser>
 20. M. Prokic, “MMM Ultrasonic Treatment,” EP 1238715A1, 2001
 21. R. Feng, Y. Zhao, C. Zhu, T.J. Mason, Enhancement of ultrasonic cavitation yield by multi-frequency sonication. *Ultrason. Sonochem.* **9**(5), 231–236 (2002). [https://doi.org/10.1016/S1350-4177\(02\)00083-4](https://doi.org/10.1016/S1350-4177(02)00083-4)
 22. V.S. Moholkar, S. Rekveld, M.M.C.G. War-moeskerken, Modeling of the acoustic pressure fields and the distribution of the cavitation phenomena in a dual frequency sonic processor. *Ultrasonics* **38**(1), 666–670 (2000). [https://doi.org/10.1016/S0041-624X\(99\)00204-8](https://doi.org/10.1016/S0041-624X(99)00204-8)
 23. P. Miodrag, “Multifrequency ultrasonic structural actuators,” EP1238715A1, Sep. 11, 2002 Accessed: Nov. 21, 2022. [Online]. Available: <https://patents.google.com/patent/EP1238715A1/zh>
 24. R. Lacoste, Chapter 10—Are You Locked? A PLL Primer, in *Robert Lacoste’s The Darker Side*. ed. by R. Lacoste (Newnes, Boston, 2010), pp.155–170. <https://doi.org/10.1016/B978-1-85617-762-7.00010-1>
 25. R.D. Christ, R.L. Wernli, *Chapter 7—Power and Telemetry* (Butterworth-Heinemann, Oxford, 2014). <https://doi.org/10.1016/B978-0-08-098288-5.00007-5>
 26. J. Grilo, V.H. Carneiro, J.C. Teixeira, H. Puga, Effect of ultrasonic melt treatment on solidification behavior of Al7SiMg alloy. *Int. J. Met.* (2022). <https://doi.org/10.1007/s40962-022-00829-2>
 27. W. Khalifa, Y. Tsunekawa, M. Okumiya, Effect of ultrasonic melt treatment on microstructure of A356 aluminium cast alloys. *Int. J. Cast Met. Res.* **21**, 129–134 (2008). <https://doi.org/10.1179/136404608X361819>
 28. M. Jolly, Prof. John Campbell’s ten rules for making reliable castings. *JOM J. Miner. Met. Mater. Soc.* **57**, 19–28 (2005). <https://doi.org/10.1007/s11837-005-0091-4>
 29. D.E.J. Talbot, Effects of hydrogen in aluminium, magnesium, copper, and their alloys. *Int. Metall. Rev.* **20**(1), 166–184 (1975). <https://doi.org/10.1179/imt.1975.20.1.166>
 30. L. Parmenter, D. Apelian, F. Jensen, Development of a statistically optimized test method for the reduced pressure test (98–18). *Trans. Am. Foundrym. Soc.* **106**, 439–452 (1998)
 31. C. Lee, Effect of ultra-sonication treatment on quality index of tensile properties of A356 aluminum alloy. *Int. J. Met.* **16**(3), 1303–1314 (2022). <https://doi.org/10.1007/s40962-021-00684-7>
 32. L. Wang, D. Apelian, M. Makhlof, *Hydrogen in Aluminum Alloy Melts: Its Sources and Its Removal* (American Foundry Society, Des Plaines, 1998)
 33. G. Sigworth, E. Williams, D. Chesonis, Gas fluxing of molten aluminum: an overview. *Essent. Read. Light Met.* **3**, 65–70 (2013). <https://doi.org/10.1002/9781118647783.ch9>
 34. V. Warke and M. Makhlof, “Hydrogen removal from molten metal mathematical modeling and computer simulations,” *Model. Cast. Weld. Adv. Solidif. Process.* vol. 2, pp. 1097–1104, 2006.
 35. J. Barbosa, H. Puga, Ultrasonic melt treatment of light alloys. *Int. J. Met.* **13**(1), 180–189 (2019). <https://doi.org/10.1007/s40962-018-0248-x>
 36. S.G. Shabestari, P. Mokarian, S. Saeidinia, Effect of process variables in rotary degassing of aluminum. *Can. Min. Metall. Bull.* **97**(1082), 74 (2004)
 37. V. Rundquist, M. Paci, R. von Gal, The development of an ultrasonic degassing process for aluminium casting. *Mater. Today Proc.* **10**, 288–295 (2019). <https://doi.org/10.1016/j.matpr.2018.10.408>
 38. T.T. Meek, Q. Han, H. Xu, Degassing of aluminum alloys using ultrasonic vibration. ORNL/TM-2006/61 (2006). <https://doi.org/10.2172/886703>
 39. J.A. Taylor, Iron-containing intermetallic phases in Al–Si based casting alloys. *Procedia Mater. Sci.* **1**,

- 19–33 (2012). <https://doi.org/10.1016/j.mspro.2012.06.004>
40. C. Lin, S. Wu, G. Zhong, L. Wan, P. An, Effect of ultrasonic vibration on Fe-containing intermetallic compounds of hypereutectic Al–Si alloys with high Fe content. *Trans. Nonferrous Met. Soc. China* **23**(5), 1245–1252 (2013). [https://doi.org/10.1016/S1003-6326\(13\)62589-3](https://doi.org/10.1016/S1003-6326(13)62589-3)
41. W. Khalifa, S. El-Hadad, Ultrasonication effects on the microstructure characteristics of the A380 die cast alloy. *Int. J. Met.* **13**(4), 865–879 (2019). <https://doi.org/10.1007/s40962-018-00296-8>
42. E. Cinkilic, M. Moodispaw, J. Zhang, J. Miao, A.A. Luo, A new recycled Al–Si–Mg alloy for sustainable structural die casting applications. *Metall. Mater. Trans. A* **53**(8), 2861–2873 (2022). <https://doi.org/10.1007/s11661-022-06711-4>
43. J. Barbosa, H. Puga, J. Oliveira, S. Ribeiro, M. Prokic, Physical modification of intermetallic phases in Al–Si–Cu alloys. *Mater. Chem. Phys.* **148**(3), 1163–1170 (2014). <https://doi.org/10.1016/j.matchemphys.2014.09.041>
44. E. Cinkilic, C.D. Ridgeway, X. Yan, A.A. Luo, A formation map of iron-containing intermetallic phases in recycled cast aluminum alloys. *Metall. Mater. Trans. A* **50**(12), 5945–5956 (2019). <https://doi.org/10.1007/s11661-019-05469-6>
45. Y. Zhao et al., 3D characterization of ultrasonic melt processing on the microstructural refinement of AlCu alloys using synchrotron X-ray tomography. *Mater. Charact.* **153**, 354–365 (2019). <https://doi.org/10.1016/j.matchar.2019.04.040>
46. S. Shivkumar, L. Wang, D. Apelian, Molten metal processing of advanced cast aluminum alloys. *JOM* **43**, 26–32 (1991). <https://doi.org/10.1007/BF03220114>
47. L. Yu, X. Liu, Z. Wang, X. Bian, Grain refinement of A356 alloy by AlTiC/AlTiB master alloys. *J. Mater. Sci.* **40**(14), 3865–3867 (2005). <https://doi.org/10.1007/s10853-005-2893-8>
48. D. Apelian, G.K. Sigworth, K. Whaler, Assessment of grain refinement and modification of Al–Si foundry alloys by thermal analysis. *AFS Transactions* **84–161**, 297–307 (1984)
49. C. Allen, Q. Han, Grain refinement of pure aluminum using ultrasonics. *Int. J. Met.* **5**(1), 69–70 (2011). <https://doi.org/10.1007/BF03355511>
50. J. Mi, D. Tan, T.L. Lee, In situ synchrotron X-ray study of ultrasound cavitation and its effect on solidification microstructures. *Metall. Mater. Trans. B* **46**(4), 1615–1619 (2015). <https://doi.org/10.1007/s11663-014-0256-z>
51. I. Tzanakis, W. Xu, G. Lebon, D. Eskin, K. Pericleous, P. Lee, In situ synchrotron radiography and spectrum analysis of transient cavitation bubbles in molten aluminium alloy. *Phys. Procedia* **70**, 841–845 (2015). <https://doi.org/10.1016/j.phpro.2015.08.172>
52. X. Dong, Y. Wang, L. Xu, Z. Liu, H. Yan, Effect of high-energy ultrasound and mixed rare earths modification on microstructure of semisolid AlSi11Cu3 alloy. *Int. J. Met.* **17**(2), 1191–1200 (2023). <https://doi.org/10.1007/s40962-022-00825-6>
53. Q. Han, Ultrasonic processing of materials. *Metall. Mater. Trans. B* **46**(4), 1603–1614 (2015). <https://doi.org/10.1007/s11663-014-0266-x>
54. H. Puga, J. Barbosa, J.M. Machado, C. Vilarinho, Ultrasonic grain refinement of die cast copper alloys. *J. Mater. Process. Technol.* **263**, 336–342 (2019). <https://doi.org/10.1016/j.jmatprotec.2018.08.034>
55. Y. Zhao, B. Lin, D. Song, D. Zheng, Z. Sun, C. Xie, W. Zhang, Effect of compound fields of ultrasonic vibration and applied pressure on the 3D microstructure and tensile properties of recycled Al–Cu–Mn–Fe–Si alloys. *Materials* **12**(23), 3904 (2019). <https://doi.org/10.3390/ma12233904>
56. Y. Zhao et al., Effect of ultrasonic melt processing and Al–Ti–B on the microstructural refinement of recycled Al alloys. *Ultrason. Sonochem.* **89**, 106139 (2022). <https://doi.org/10.1016/j.ultsonch.2022.106139>
57. Y. Zhao et al., Effect of ultrasonic treatment and squeeze casting on the microstructural refinement of Al–Cu–Mn alloys. *Int. J. Met.* (2023). <https://doi.org/10.1007/s40962-023-01092-9>
58. G. Liang, Y. Ali, G. You, M.-X. Zhang, Effect of cooling rate on grain refinement of cast aluminium alloys. *Materialia* **3**, 113–121 (2018). <https://doi.org/10.1016/j.mtla.2018.08.008>

Publisher's Note Springer Nature remains neutral with regard to jurisdictional claims in published maps and institutional affiliations.